

Medical Biophysics: cancer growth, heart electrophysiology

Jean Bragard

*Department of Physics and Applied Mathematics,
&*

*Institute of Data Science and Artificial Intelligence,
University of Navarra.*

31008 Pamplona. SPAIN.



Universidad
de Navarra

I) Tumor growth dynamics

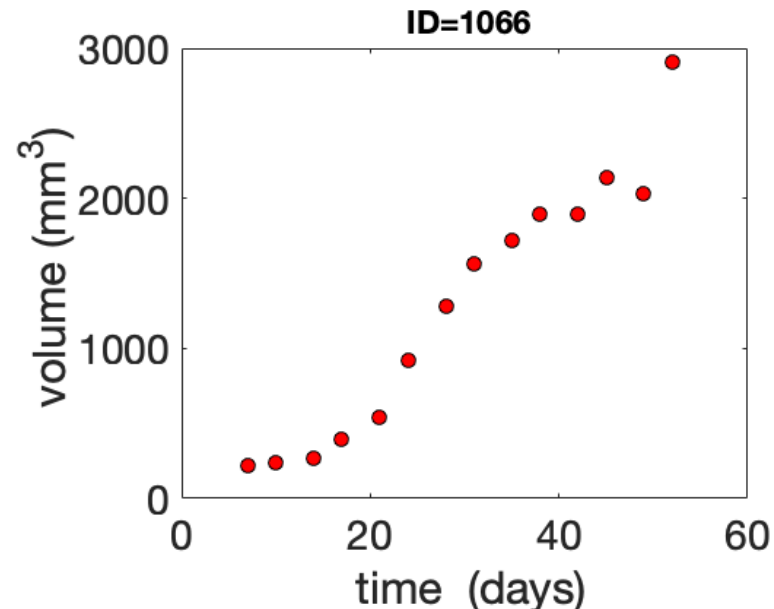
Tumor growth modeling (TGM)



We have access to numerous data of the tumor's evolution.
The tumor volume is measured by a caliper technique over time.

Interest of the model for

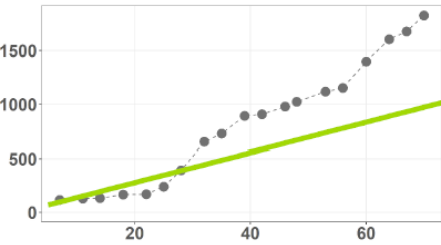
1. Disease (unperturbed tumor) progression
2. Treatment effects



TGM: “classical” models

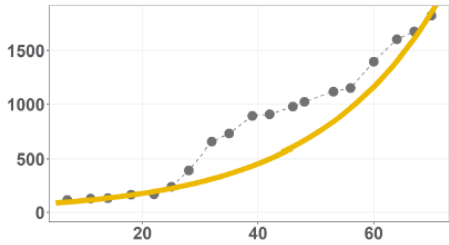
$$\frac{dTS}{dt} = \lambda$$

Lineal Model



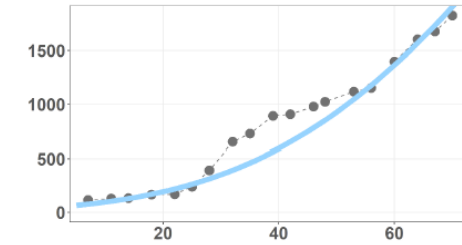
$$\frac{dTS}{dt} = \lambda \times TS$$

Exponential Model



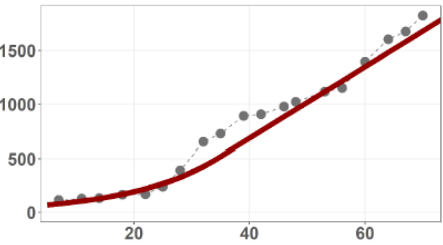
$$\frac{dTS}{dt} = \alpha \times TS \times \log\left(\frac{TS_{max}}{TS}\right)$$

Gompertz Model



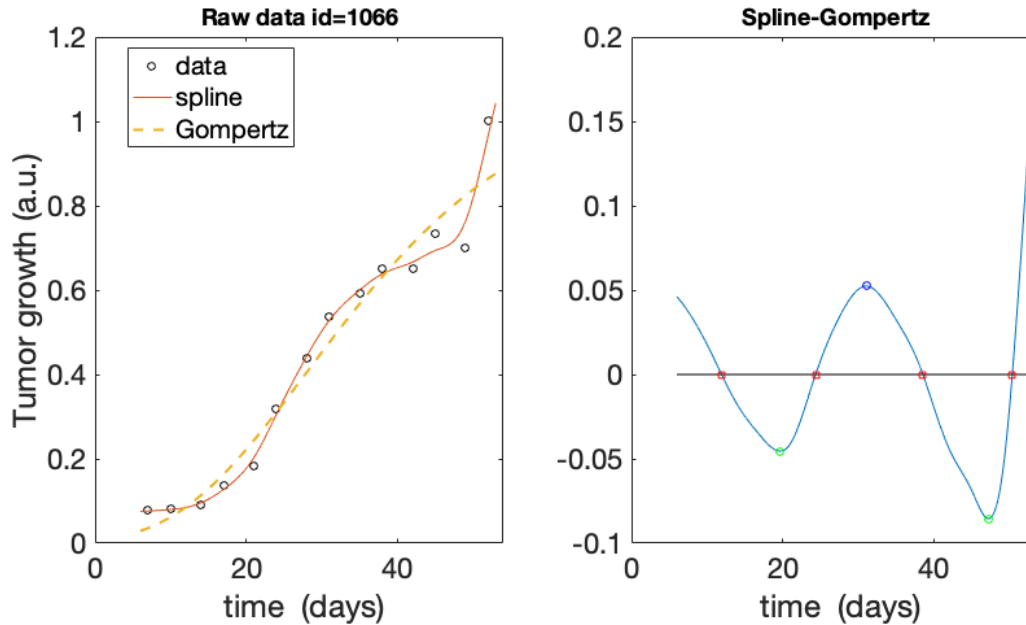
$$\frac{dTS}{dt} = \frac{\lambda_o \times TS}{\left\{1 + \left[\left(\lambda_0/\lambda_1\right) \times TS\right]^\psi\right\}^{1/\psi}}$$

Simeoni Model



Classical models for tumor growth are monotonic and the data seem to indicate that the growth could be oscillatory.

Data exploration (use splines)

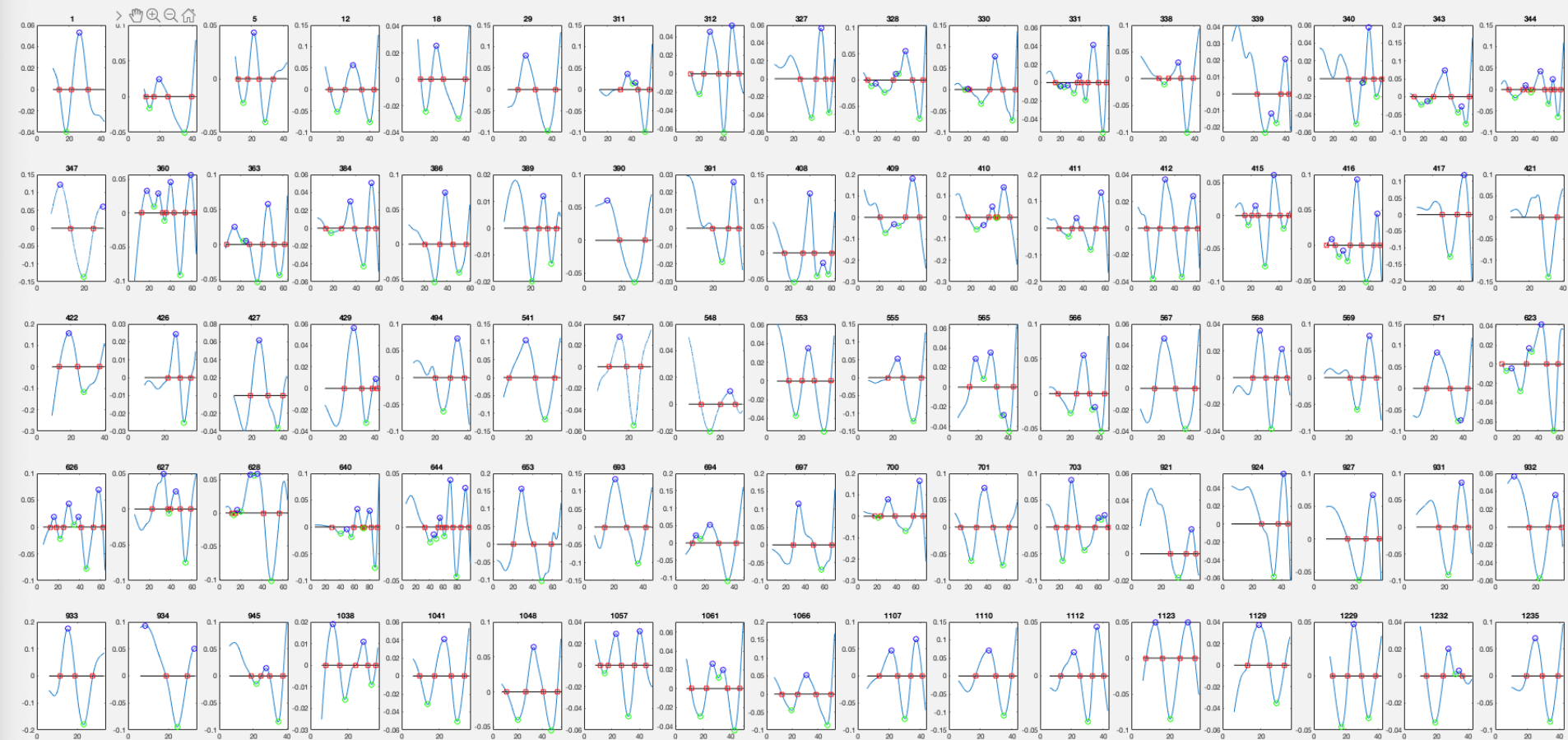


First we explore a purely empirical model based on the **cubic spline fitting** of the data.

We compare the spline with the best classical fit, i.e., logistic, exponential or Gompertz.

From the residuals, we compute the “half period” of the oscillations.

Data exploration (85 data, 6 tumor types)



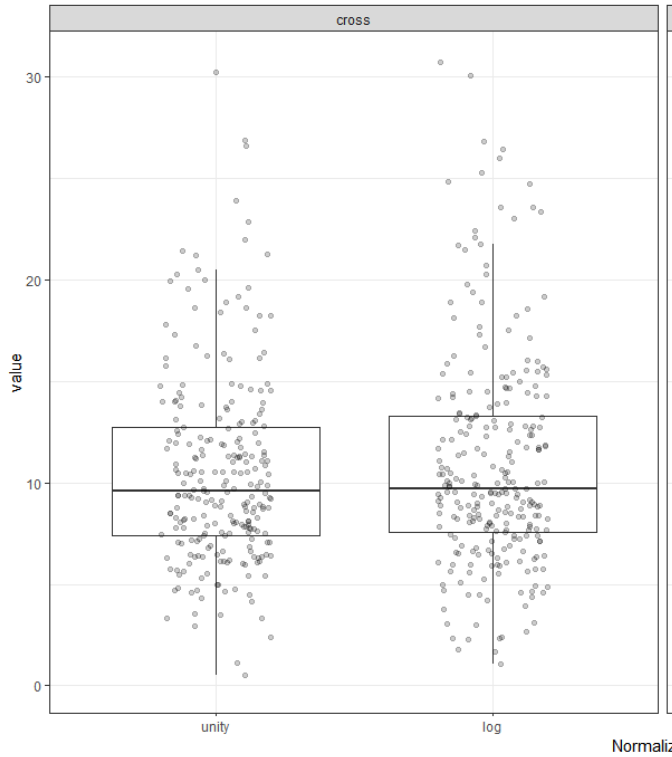
We compute the half-periods in four different ways:

Zero-crossings of residuals (when data are normalized with unity and log scale);

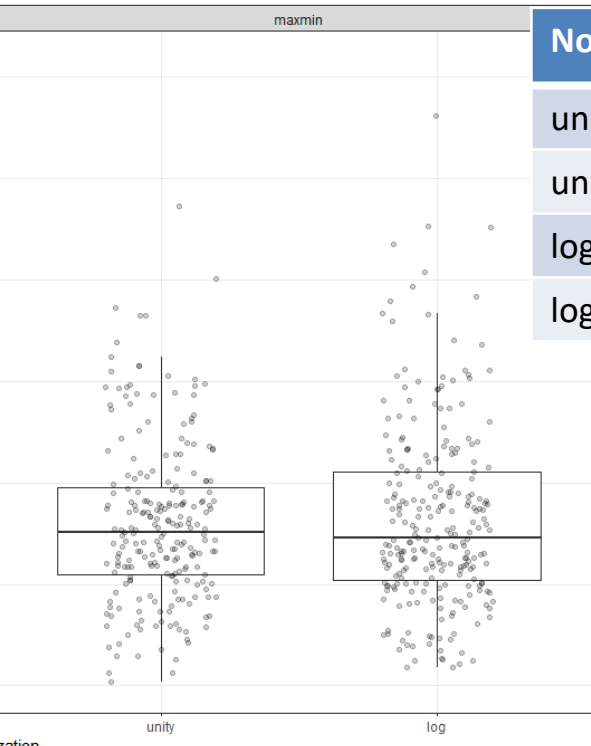
Successive extrema of the residuals (for data normalized with unity and log scale).

Empirical half periods

zero-crossings



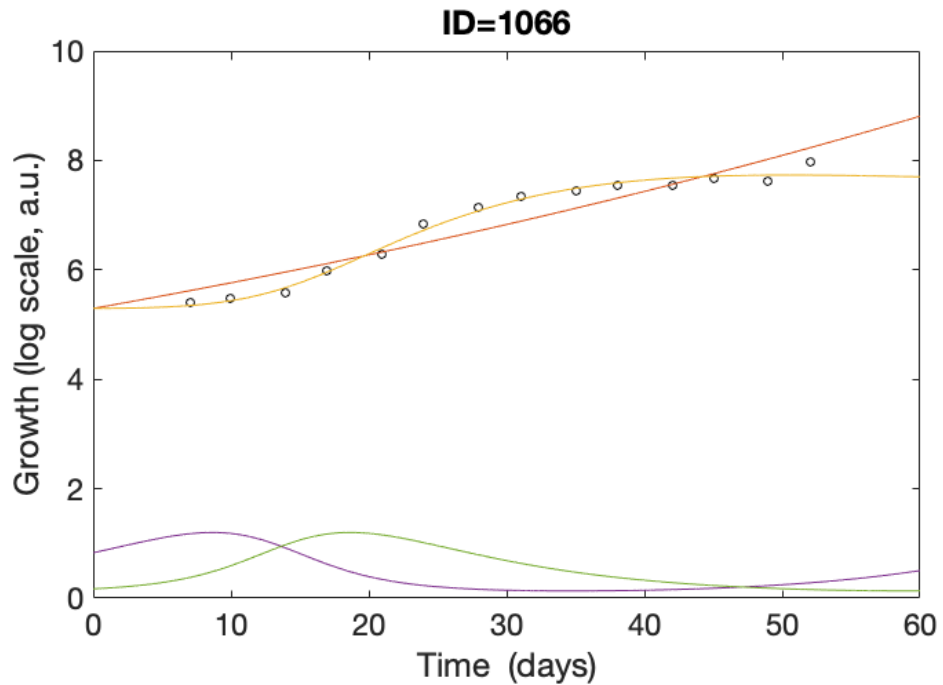
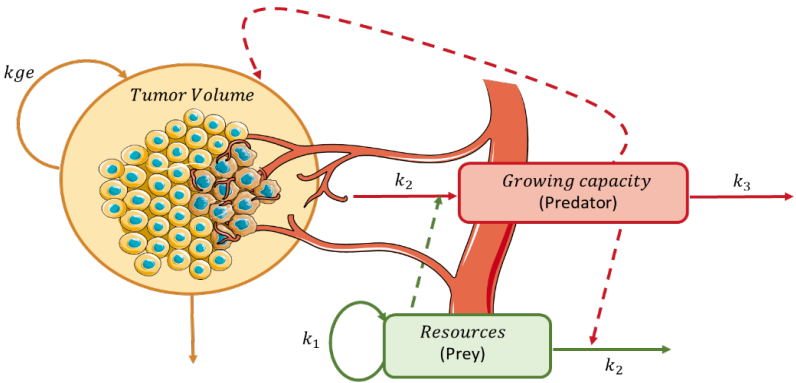
extrema



Normalization	HPs	mean	sd
unity	cross	10.5	4.72
unity	maxmin	8.00	3.95
log	cross	10.9	5.32
log	maxmin	8.25	4.47

Collecting all the available data, we observe that the median values for the half-periods are in the 8 to 10 days range.

An oscillating model for tumor growth



We combine a prey-predator model with a classical exponential growth to produce an oscillating model.

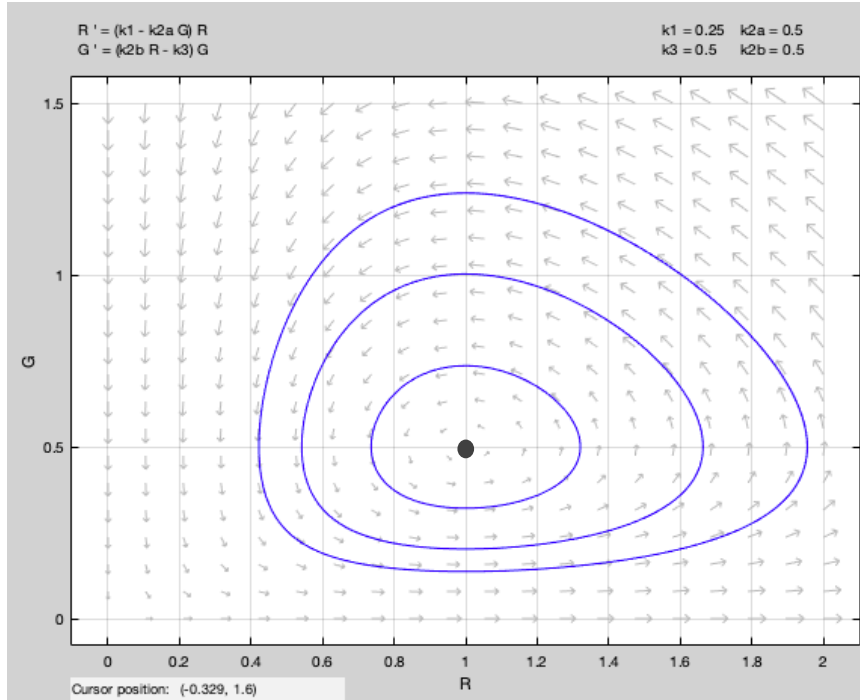
The new model (3 ODEs) is able to fit the data nicely.

$$\frac{dT}{dt} = k_{ge} T G - k_{death} T \quad \text{Tumor vol.}$$

$$\frac{dR}{dt} = k_1 R - k_2 R G \quad \text{Prey}$$

$$\frac{dG}{dt} = k_2 R G - k_3 G \quad \text{Predator}$$

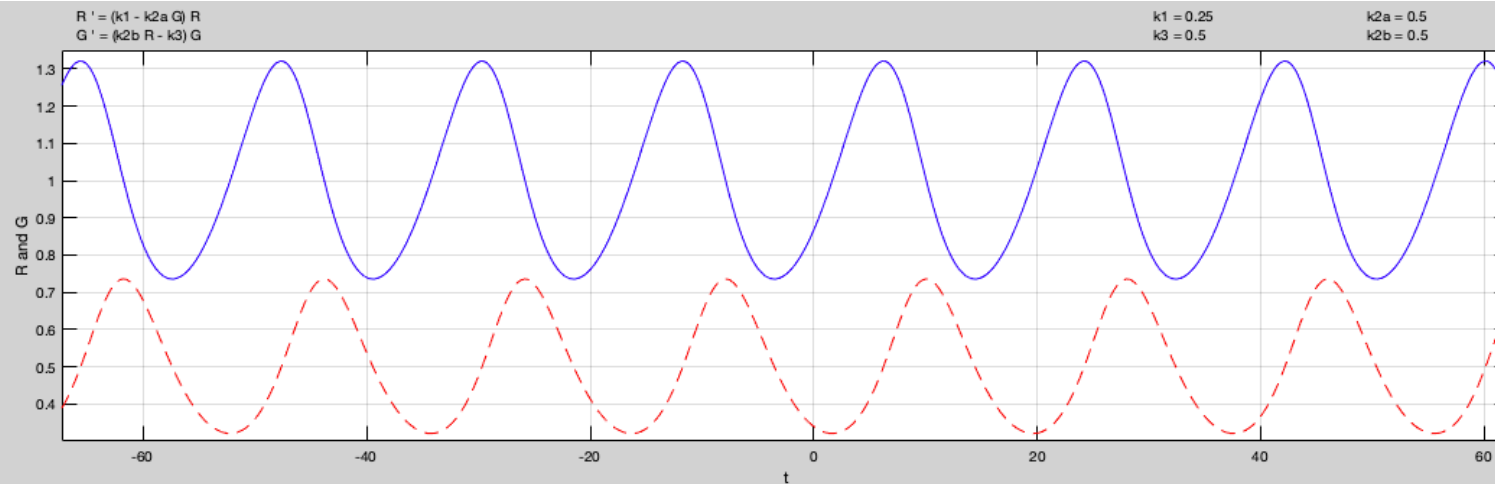
Prey (R) – Predator (G) dynamics



$$\frac{dR}{dt} = k_1 R - k_2 R G$$

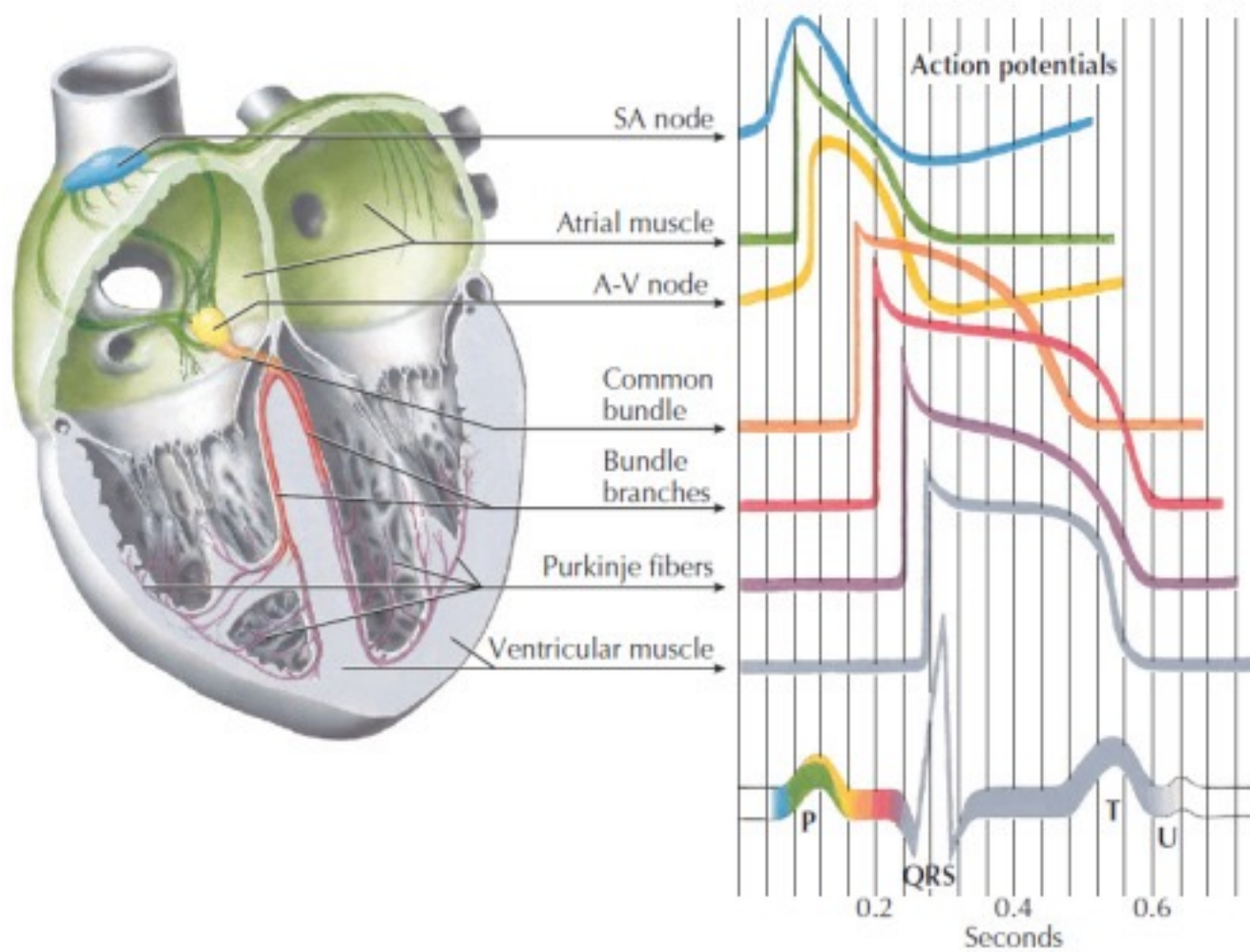
$$\frac{dG}{dt} = k_2 R G - k_3 G$$

$$G_{eq} = \frac{k_1}{k_2} \quad R_{eq} = \frac{k_3}{k_2}$$

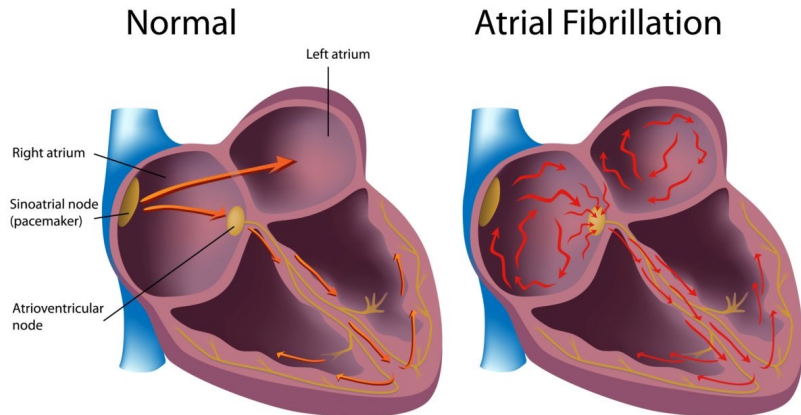


II) Atrial fibrillation

Cardiac conduction system and its relation with the ECG



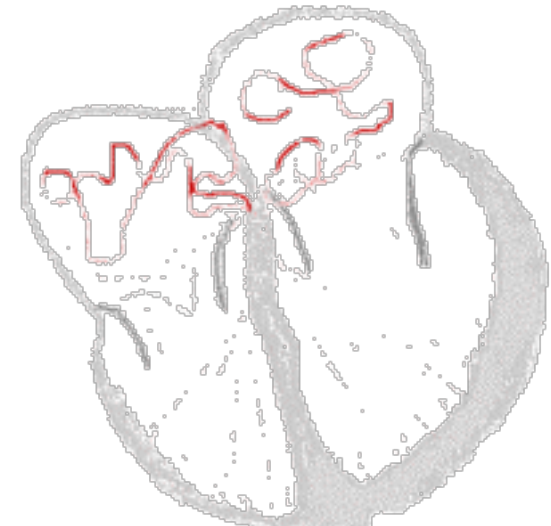
Atrial fibrillation (Afib)



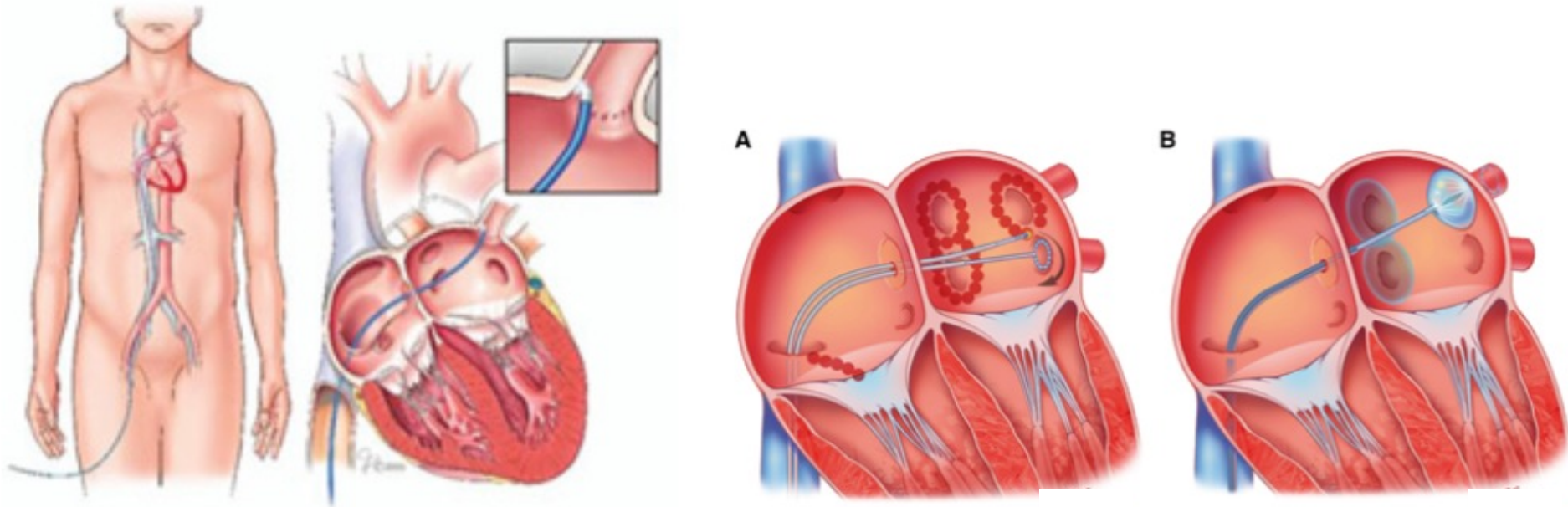
We have studied images that corresponds to Afib patients (left atrium)

1. Pathophysiology
2. Predictive power.

Afib is an arrhythmia that does not present a direct risk for the patient's life (the fluid fills the ventricles anyway). But in the long run, a thrombus may form in the atrium and sometimes travels to the brain and cause a stroke.



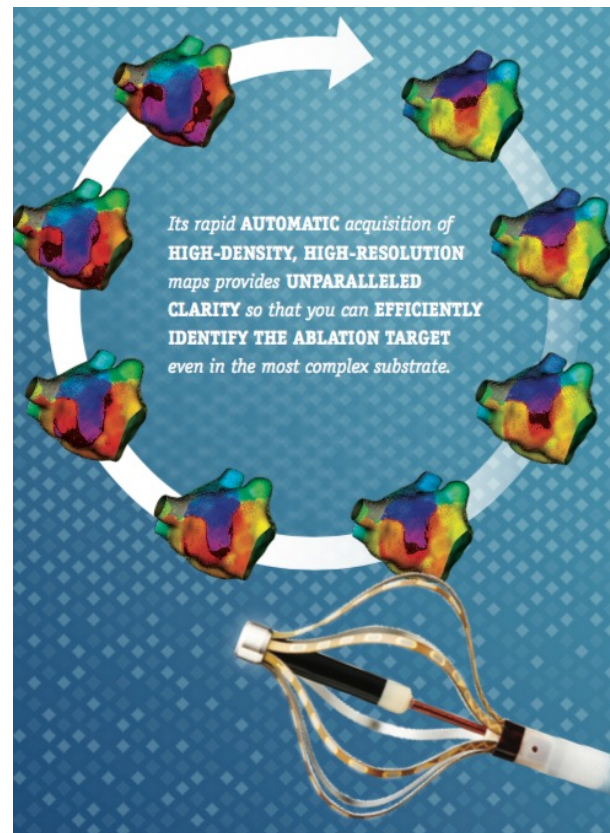
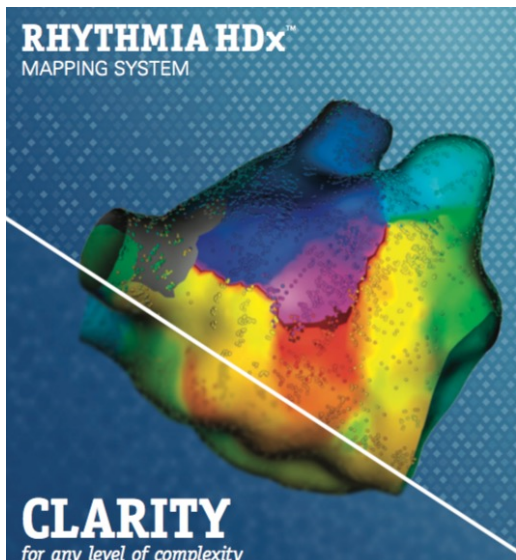
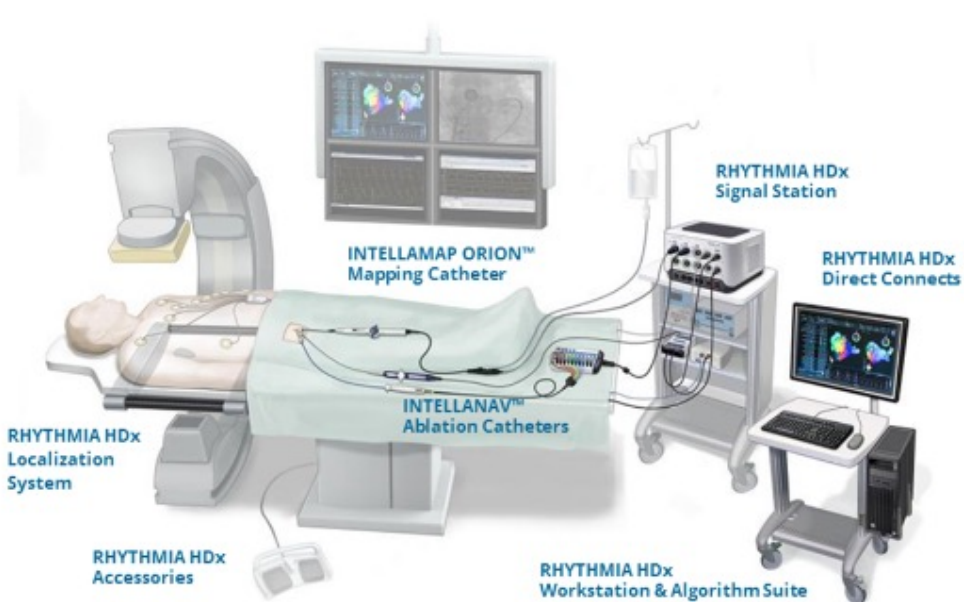
Clinical solution to Afib is to ablate the re-entry circuit and essentially the PVs



~30% of the ablation procedures will fail (Afib presents after 1 year follow-up)
Two main techniques are used: radiofrequency ablation (A) and cryoablation (B).
+Blood thinners (anticoagulation therapy) to prevent blood clots from forming.

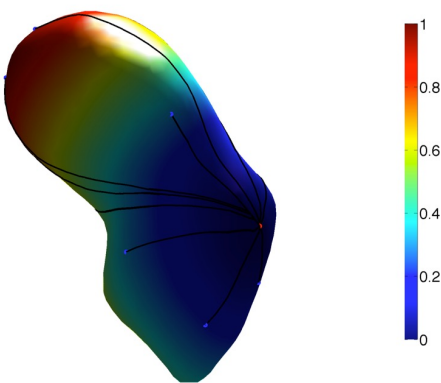
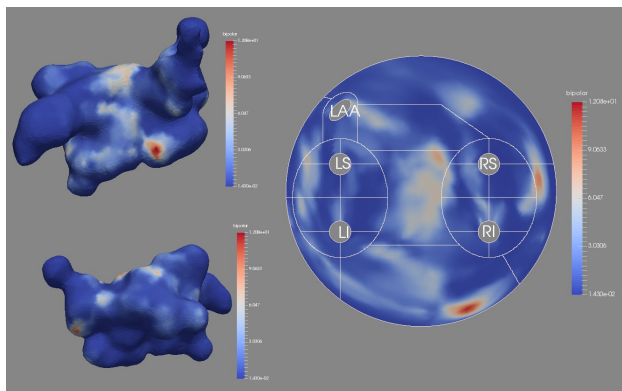
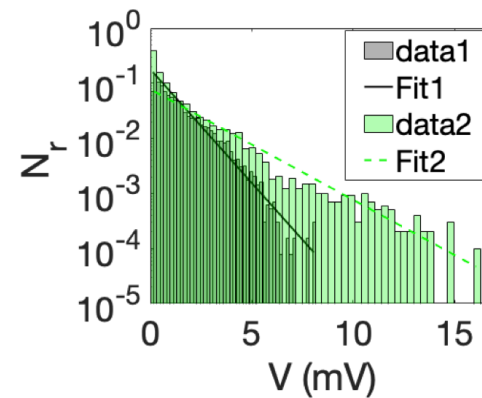
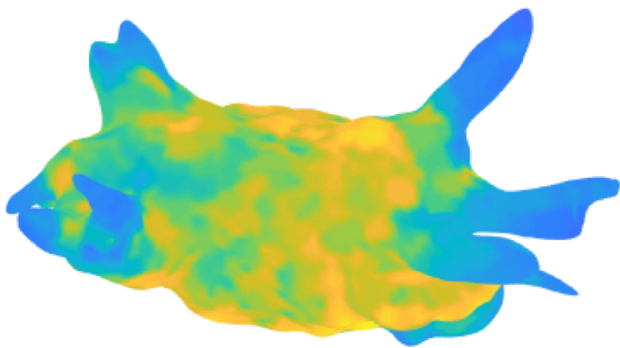
System used prior to ablation to map the patient left atrium

Rhythmia system (Boston scientific)



Activation time mapping,
and bipolar/unipolar electrogram voltage maps are acquired
(~20 min/patient)
The data are saved in a readable Matlab format for analysis

Electrical biomarkers are evaluated from the bipolar maps



Two electrical biomarkers:

1. Mean voltage $\langle V \rangle$
2. Slope of the histogram (VS)

Future:

- 24 regions of the atrium (regional statistics)
- Geodesic distance on the time activation maps (PhD thesis Leire Moriones)

We studied 122 patient maps (prior to ablation)

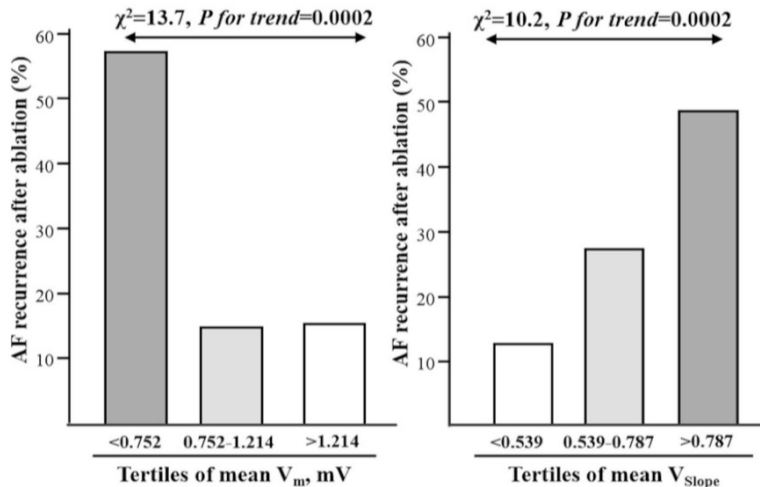
	A	B	C	D	E	F	G	H	I	J	K	L	M	N	O	P	Q	R	S	T				
1	name	NVERT	NFACES	AREA	MEDIA POT	Slope	R2	False media	dispersion	Q1	Q2	Q3												
2	pot<0,1	P<0,2	P<0,3	P<0,4	P<0,5	P<0,6	P<0,7	P<0,8	P<0,9	P<1	P<1,1	P<1,2	P<1,3	P<1,4	P<1,5	P<1,6	P<1,7	P<1,8	P<1,9	P<2				
3																								
4	F01_12_2015T09h08	7357	14513	137.3	0.7143	-0.9682 (0.0302)	0.956	0.7155 (0.912)	0.9460 (0.349)	0.1416	0.3492	0.9248												
5		0.1654	0.3522	0.4587	0.5387	0.6017		0.6494	0.6863		0.7168		0.7434	0.7668	0.7869	0.8059	0.8218	0.8375	0.8534	0.8661	0.8805	0.8914	0.9006	0.9103
6																								
7	F03_11_2015T09h58	7828	15470	145.31	1.0769	-0.4961 (0.0203)	0.926	1.0618 (1.587)	0.9393 (0.357)	0.1312	0.3573	1.4863												
8		0.1925	0.3767	0.4603	0.5219	0.566		0.5972	0.6222		0.6418		0.6607	0.6807	0.6979	0.7136	0.728	0.7406	0.7513	0.7634	0.7773	0.7869	0.7997	0.8109
9																								
10	F04_08_2015T13h08	7795	15440	147.52	0.1869	-1.8882 (0.1251)	0.847	0.1809 (0.290)	0.9554 (0.363)	0.0428	0.0801	0.1922												
11		0.5809	0.7589	0.8346	0.879	0.9091		0.9306	0.945		0.9562		0.9659	0.9727	0.9778	0.9815	0.9842	0.9873	0.9902	0.9926	0.994	0.9948	0.9965	0.9979
12																								
13	F05_11_2015T09h20	5068	9955	97.15	1.1941	-0.4625 (0.0208)	0.92	1.1807 (1.669)	0.9759 (0.361)	0.176	0.5399	1.5004												
14		0.1339	0.2749	0.3693	0.4337	0.484		0.5231	0.5619		0.5929		0.6297	0.6543	0.6787	0.7002	0.7175	0.7323	0.7499	0.7612	0.7743	0.7877	0.7999	0.8112
15																								
16	F09_09_T08h49	6989	13832	137.41	0.8219	-0.7329 (0.0289)	0.933	0.8191 (1.198)	0.9934 (0.375)	0.1176	0.2619	1.1075												
17		0.1674	0.4429	0.5233	0.5807	0.6235		0.6552	0.6803		0.702		0.7188	0.7336	0.7493	0.765	0.7784	0.7923	0.807	0.8199	0.8308	0.8419	0.8539	0.8652
18																								
19	F17_11_T14h51	7539	14836	143.93	2.0659	-0.4578 (0.0134)	0.96	2.0679 (2.401)	0.9701 (0.351)	0.1938	1.2555	3.033												
20		0.185	0.2531	0.3003	0.3326	0.357		0.3786	0.3998		0.419		0.4358	0.4559	0.4726	0.4896	0.5073	0.5252	0.5419	0.5584	0.5745	0.5904	0.6096	0.6245
21																								

Working hypotheses:

- 1) Low voltage areas correlate with scar tissue areas (see LGE-MRI studies)
- 2) Scar tissue (fibrosis) is prone to generate re-entry (arrhythmogenic substrate)
- 3) Heavily damaged LA is more susceptible to lead to “redo procedure” (probability)

→ Average potential and slope are the two “electrical” biomarkers of the LA !

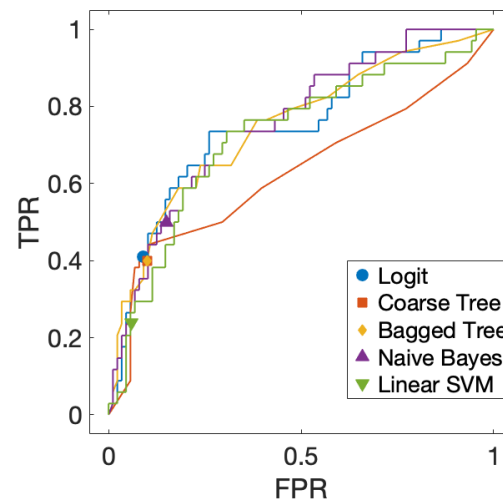
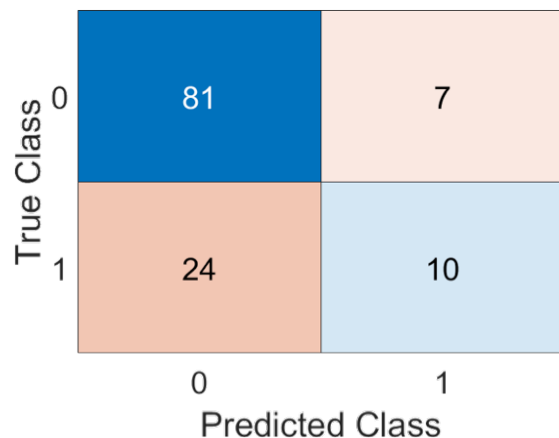
Main results of the map analysis



Results:

Both mean voltage (V_m) and VS are predictors of AF recurrence after ablation !

Logistic Regression is the best classifier given by the Matlab “classificationLearner” ML tool, (with a cutoff value of $V_m = 0.54$ mV).



Redo: 34/122 ≈ 28 %; Accuracy ≈ 75 %

Partial conclusions

- The average potential and the slope are good predictors for a repeat procedure at one year distance.
- More complicated statistical indicators are currently being tested,i.e., regional statistics and activation time maps.



ORIGINAL ARTICLE

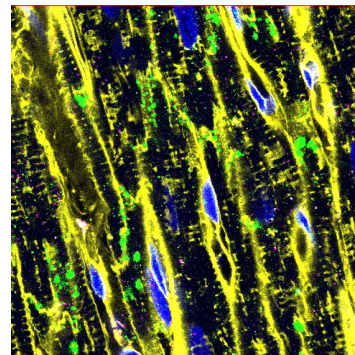
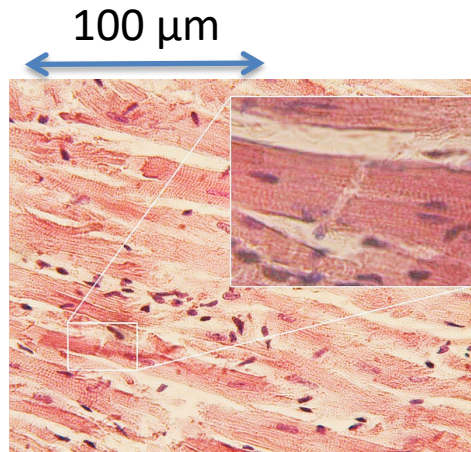
Association of left atrium voltage amplitude and distribution with the risk of atrial fibrillation recurrence and evolution after pulmonary vein isolation: An ultrahigh-density mapping study

Gabriel Ballesteros MD, Susana Ravassa PhD, Jean Bragard PhD, Pablo Ramos MD, Begoña López PhD, Enrique Vives MD, Renzo Neglia MD, Bernardo Wise MD, Arantxa González PhD ... See all authors ▾

First published: 11 May 2019 | <https://doi.org/10.1111/jce.13972>

III) Wave propagation in the heart

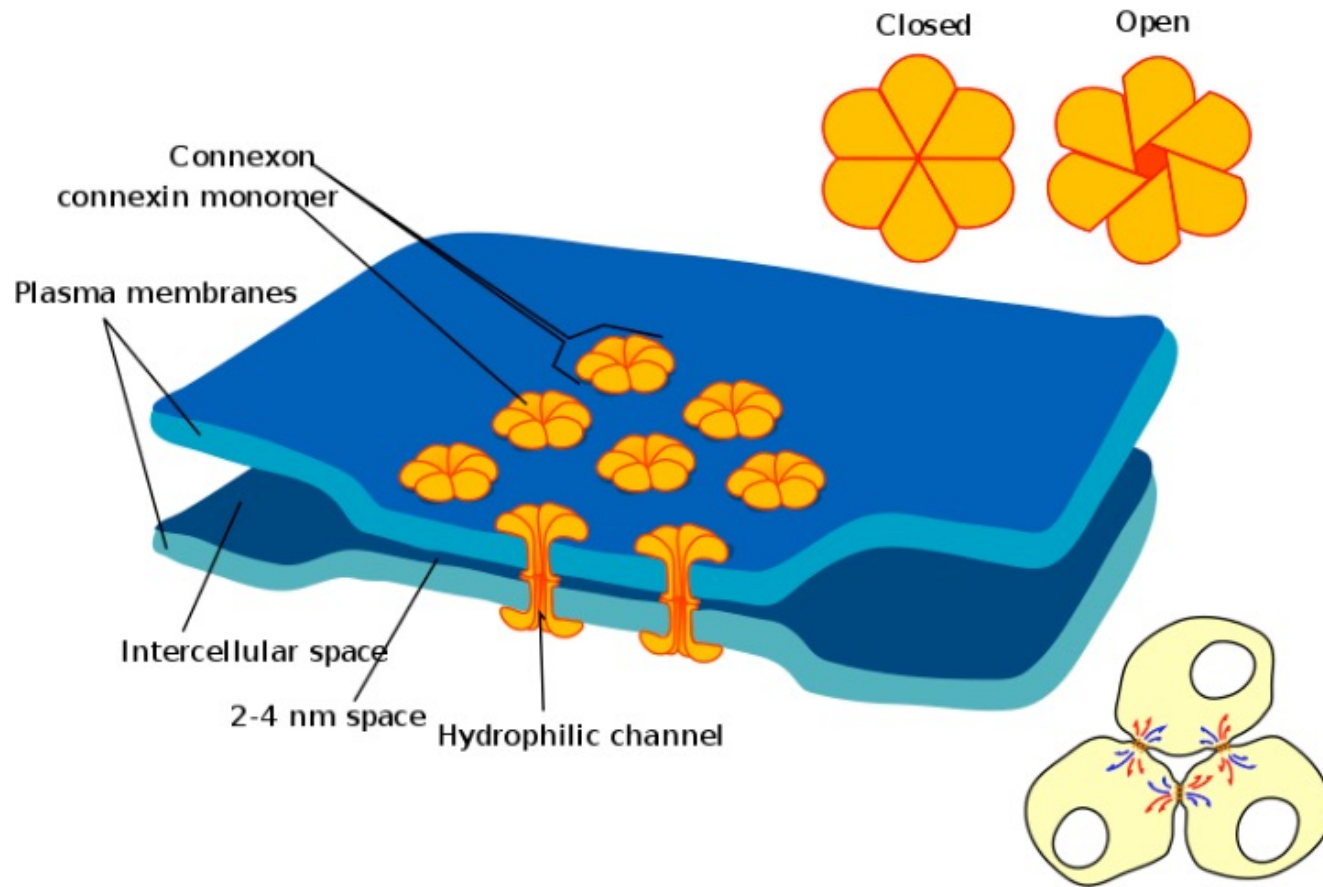
The structure of the cardiac muscle is complex and influences its electrical behavior and dynamics



- Wheat Germ Agglutinin (WGA)
- DAPI
- GJ (Connexin43)

The cardiac muscle is formed with cardiomyocytes, gap junctions (GJ), collagen and elastin fibers, fibroblasts, blood vessels,...

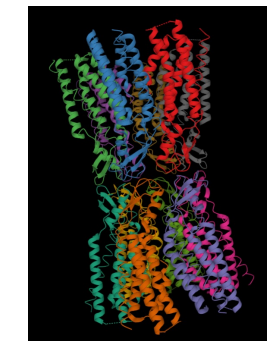
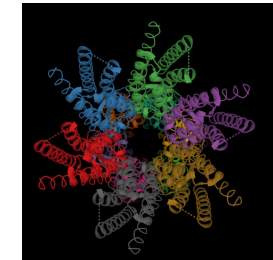
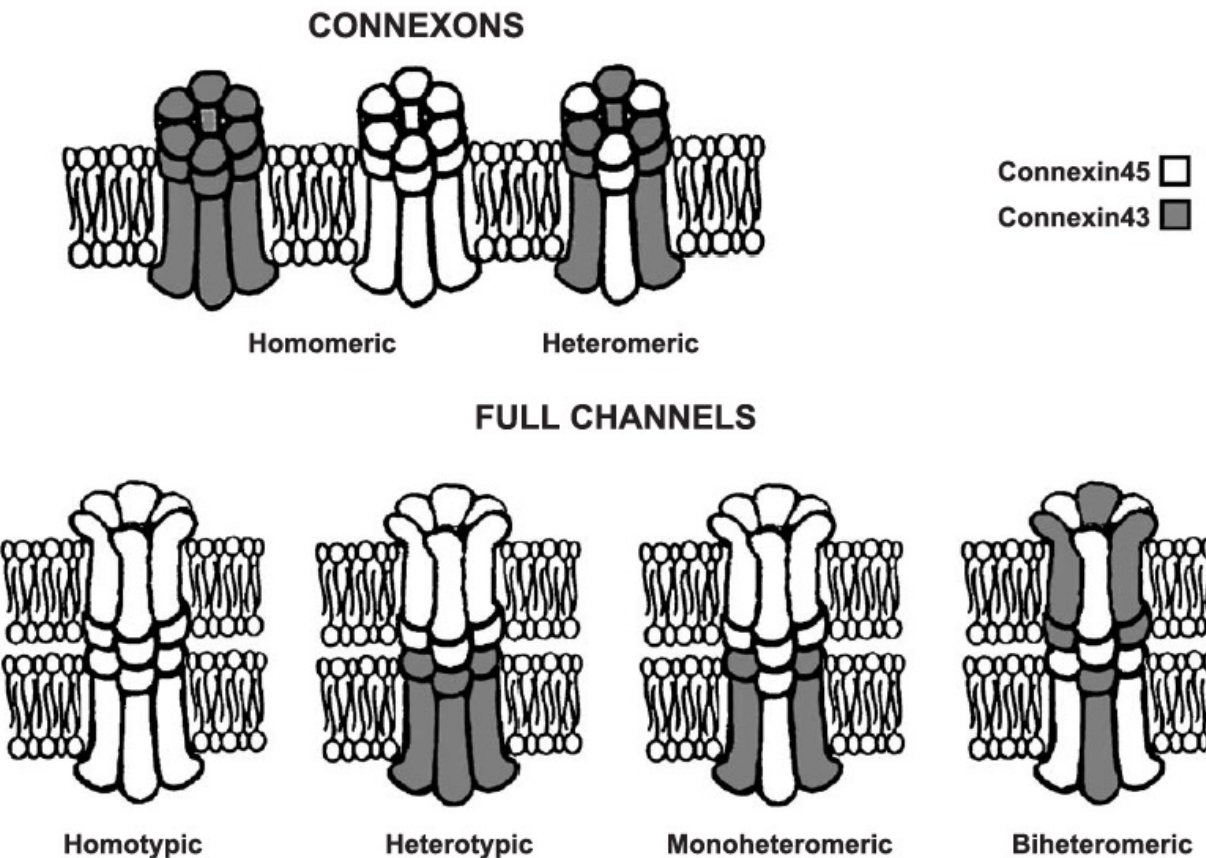
Gap junctions (GJ) are essential for the propagation of the electrical impulse AP from one myocyte to the next.



GJs form low electrical resistance passages between cardiomyocytes.

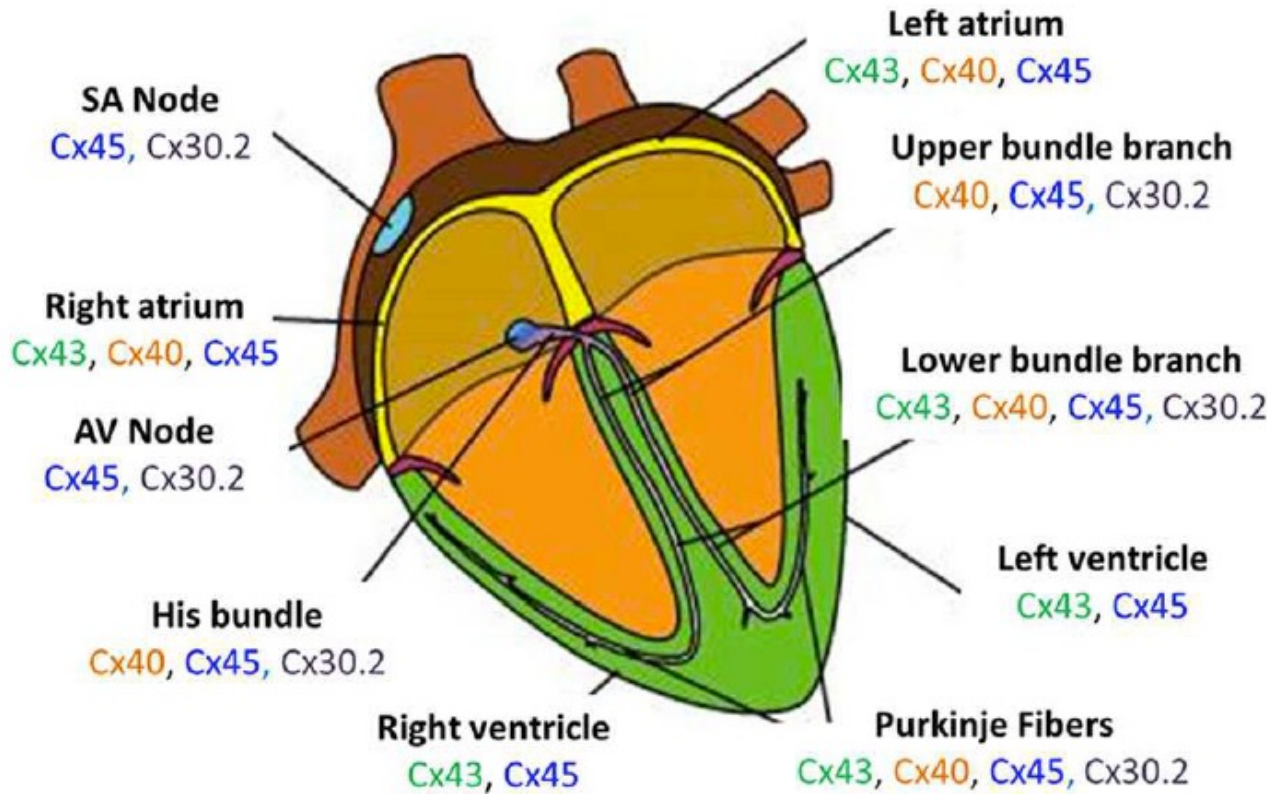
Source : Wikipedia

Different types of gap junctions (GJ) have been identified in the cardiac muscle



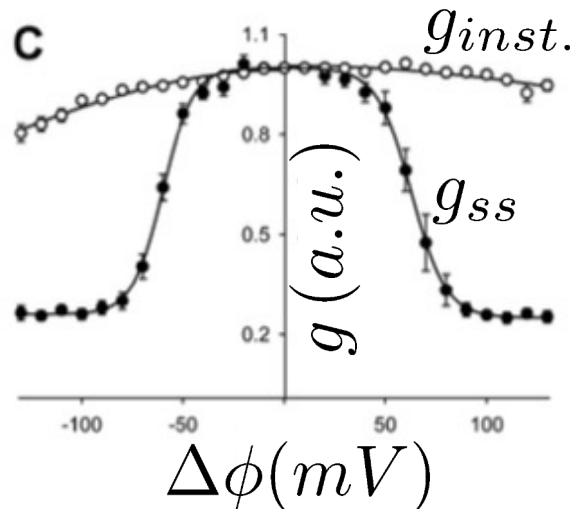
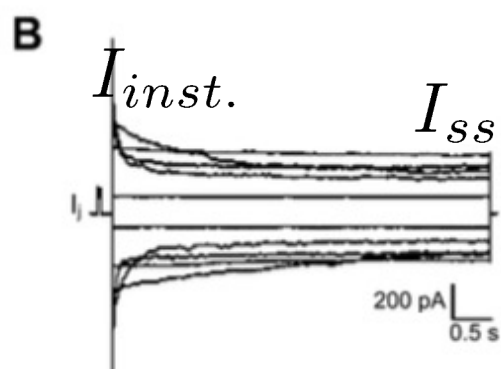
In cardiac tissue of mammalian, connexins type Cx40, Cx43 and Cx45 are the most common. The permeability of the GJ depends on its structure (g approx. 10 to 300 pS)

Different types of gap junctions (GJ) have been identified in the cardiac muscle (II)



The connexin's expression pattern varies in different location of the heart

Dual voltage-clamp method and whole-cell recording allow to measure the electrical properties of the GJ



a) Fix the membrane potential of both cells

$$\Delta\phi = V_2 - V_1 \quad \text{transjunctional voltage}$$

b) Measure the current between cells

$$I_{inst.} \quad I_{ss}$$

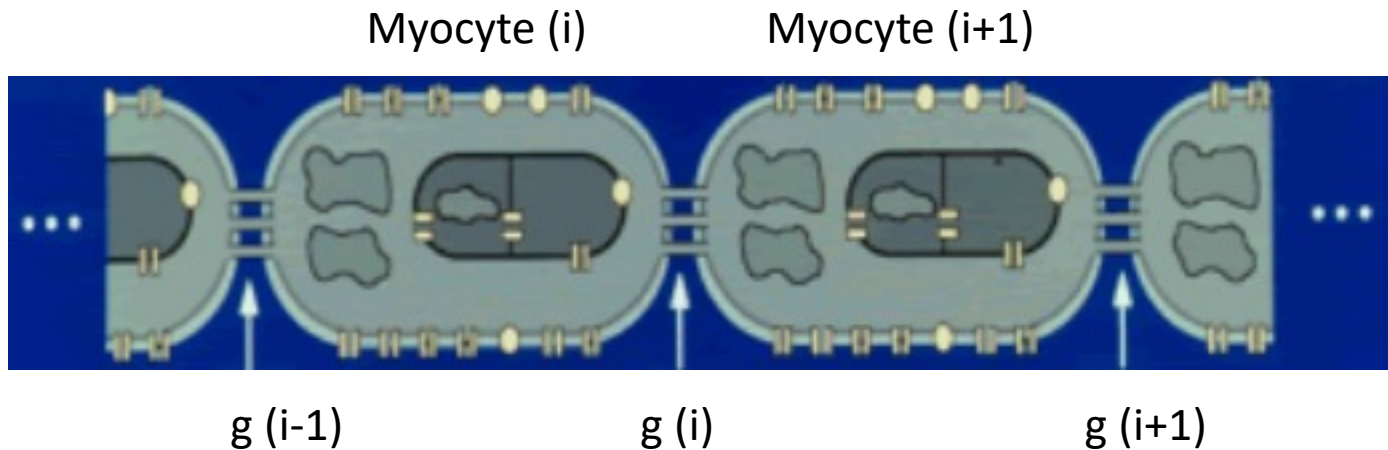
c) Calculate the normalized conductances

$$g_{inst.} = I_{inst.}/\Delta\phi \sim 100 \text{ } pS$$

$$g_{ss} = I_{ss}/\Delta\phi$$

The conductance between the two cells is a **dynamical variable**.

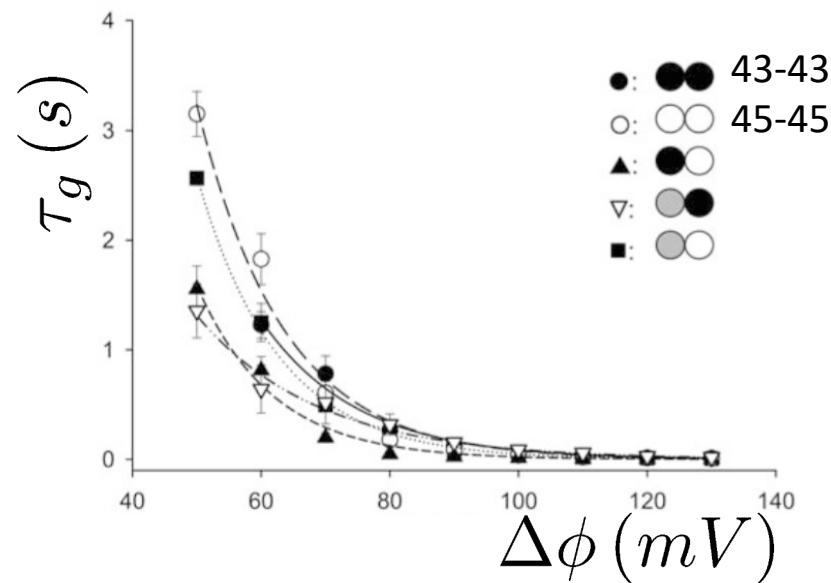
Mathematical model of a strand of cardiac tissue



1) Gap Junction's dynamics

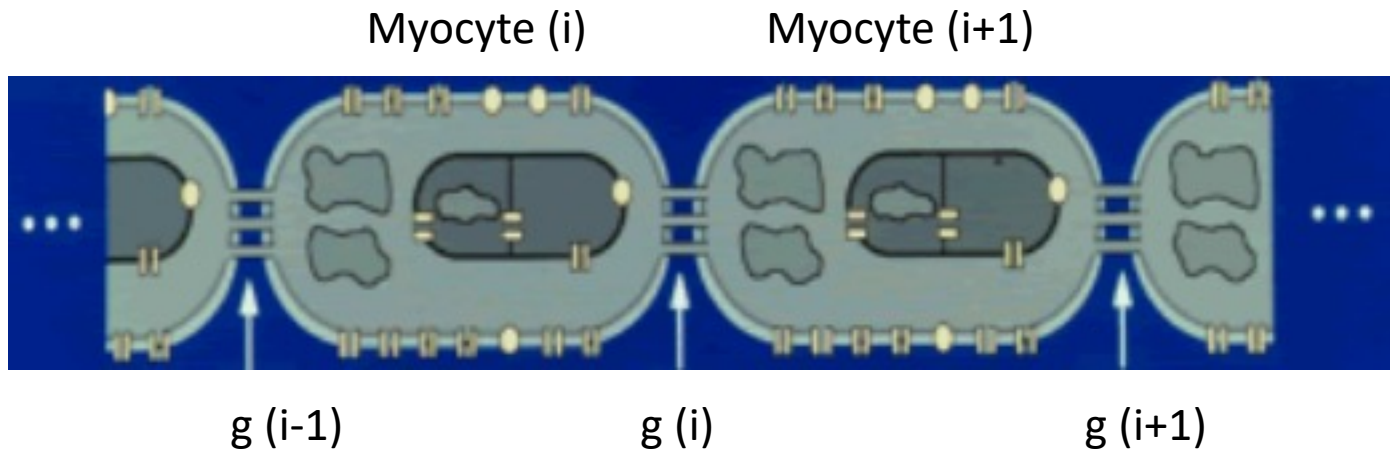
$$\frac{dg_i}{dt} = \frac{g_{ss}(\Delta\phi_i) - g_i}{\tau_g(\Delta\phi_i)}$$

$$\Delta\phi_i = V_{i+1} - V_i$$



The time constant τ_g is highly dependent of the connexin's transjunctional voltage

Mathematical model of a strand of cardiac tissue (ii)



2) Myocyte's transmembrane dynamics

$$\frac{\partial V}{\partial t} + \frac{I_{myo} + I_{ext}}{C} = \nabla \cdot (D \nabla V)$$

$$\frac{\partial \mathbf{s}}{\partial t} = f(V, \mathbf{s}) \quad \text{5 variables model (BCN)}$$

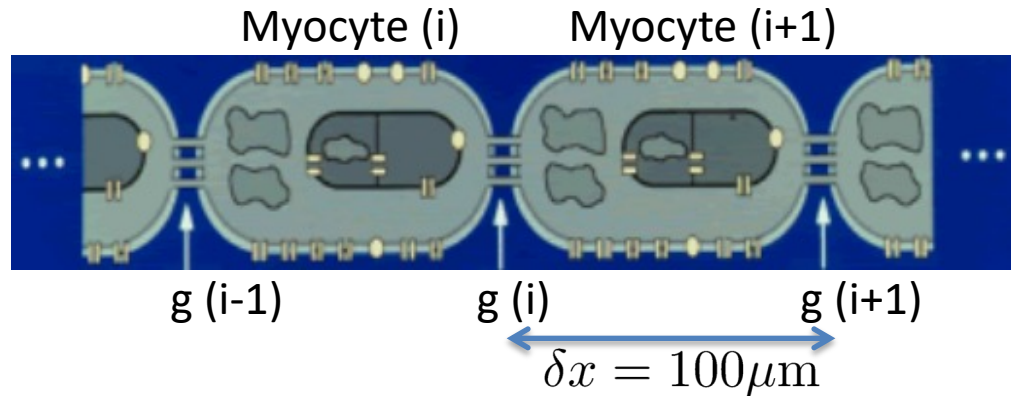
$$V = \phi_{intra} - \phi_{extra}$$

Monodomain approximation

$$D(x, t) = \bar{D} g(x, t)$$
$$\bar{D} = 1.5 \text{ cm}^2/\text{s}$$

- The gap junctions are the primary sites of membrane potential changes
- The entire myocyte cytoplasm becomes effectively iso-potential.

Numerical method



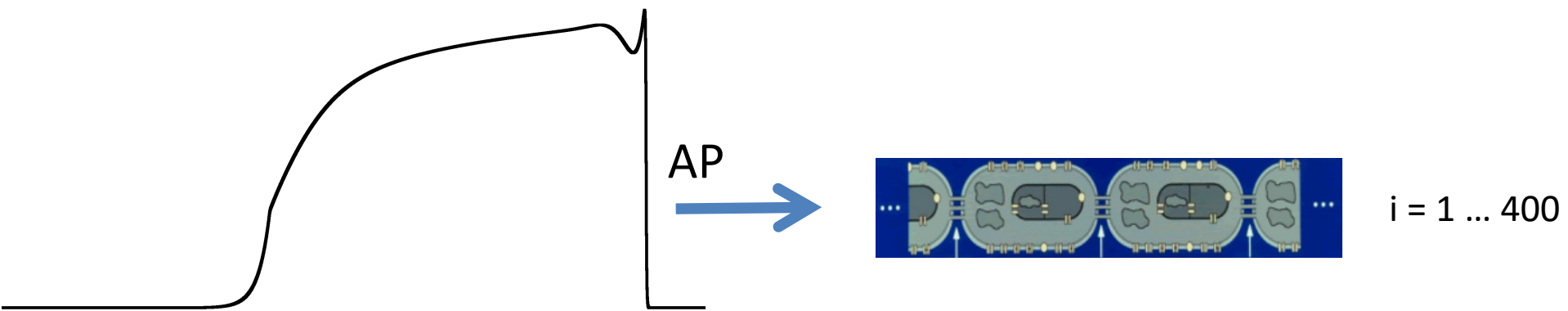
$$V_i^{(n+1)} = V_i^{(n)} + \bar{D} \frac{\delta t}{\delta x^2} \left\{ g_i^{(n)} \left[V_{i+1}^{(n)} - V_i^{(n)} \right] - g_{i-1}^{(n)} \left[V_i^{(n)} - V_{i-1}^{(n)} \right] \right\} - \delta t \frac{I_{myo}^{(n)} + I_{ext}^{(n)}}{C}$$

$$g_i^{(n+1)} = g_i^{(n)} + \delta t \frac{g_{ss}(\Delta\phi_i^{(n)}) - g_i^{(n)}}{\tau_g(\Delta\phi_i^{(n)})}$$

$\delta t = 10\mu\text{s}$ Integration time step

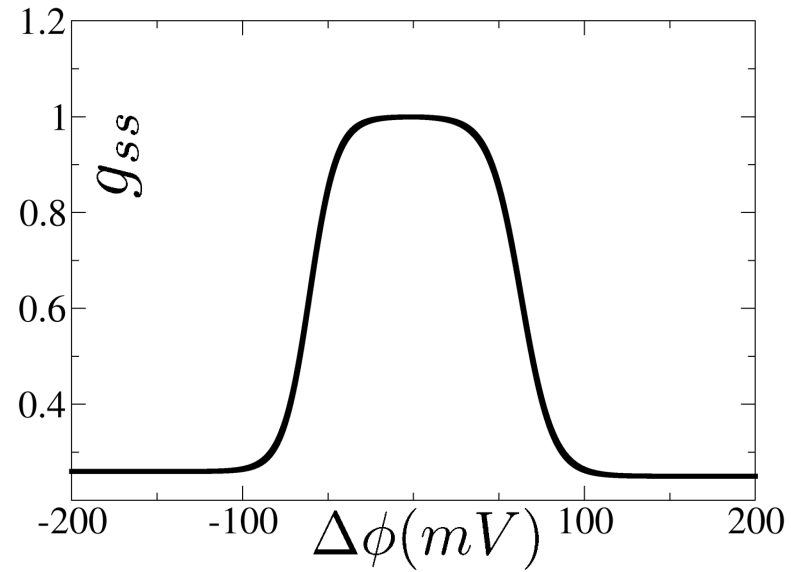
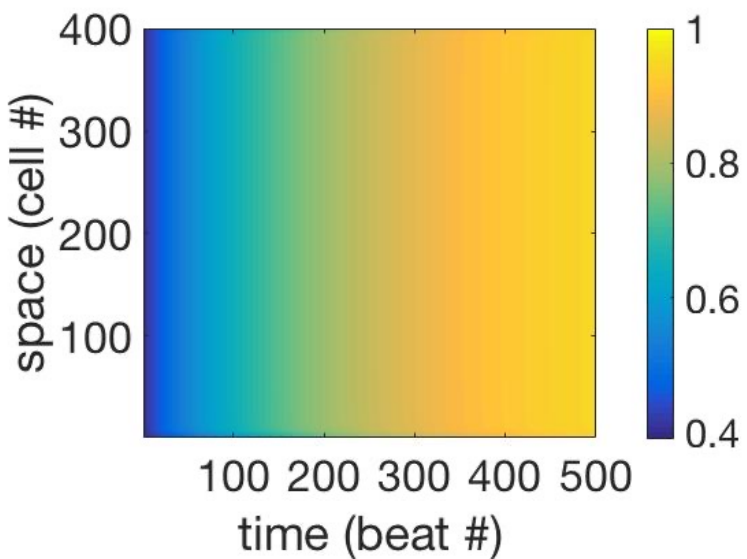
Super-index (n) refers to time step n. Subscript i refers to position i in the chain.

Stimulation protocol (L=400 cells)



1. Same initial values are set to all the GJ conductances ($g_i = g_{ini}$)
2. We excite the first 7 cells ($i=1..7$) to elicit an AP that propagates through the fiber
3. We repeat the stimulation with a period of $T = 480$ ms
4. We measure the time evolution of the GJ conductances after each stimulation

Results for the normal case (healthy)

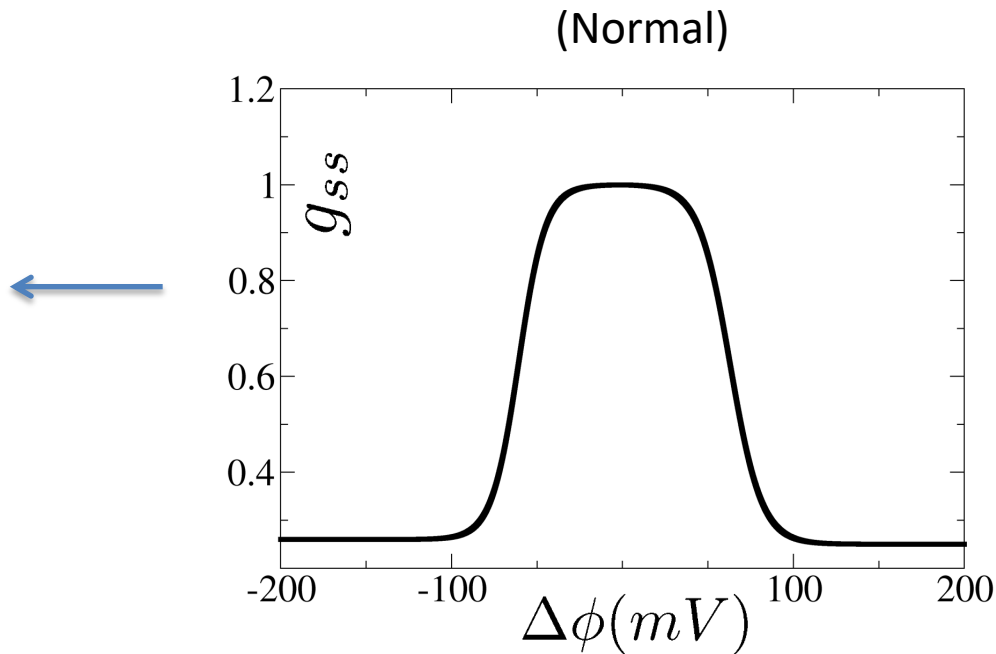
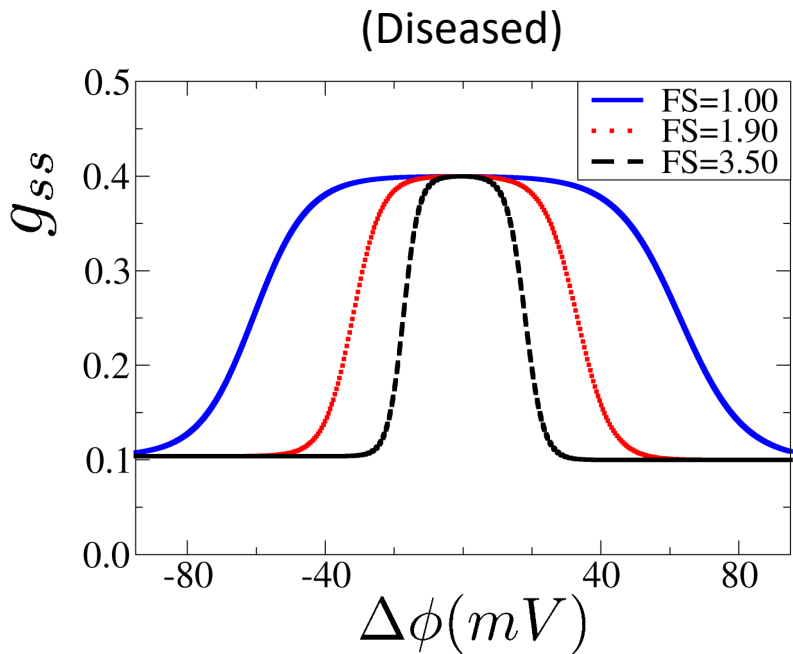


Here we set $g_{ini} = 0.4$

The conductances of all the GJ are returning to the max value $g \sim 1$

Nothing fancy happens !

Modification of the GJ dynamics (diseased case)

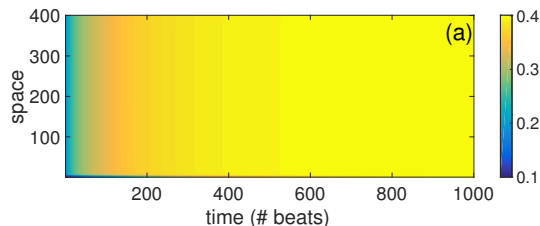


In order to model a diseased tissue we modify the characteristics of the GJ

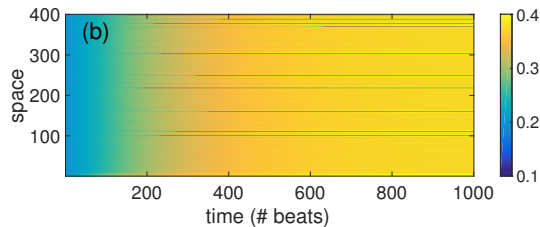
- We reduce the overall conductance to 40% of the normal values (ischemia)
- We introduce the ‘shrinking factor’ FS that alters the width of the plateau

Results of the GJ bistability induced by varying FS

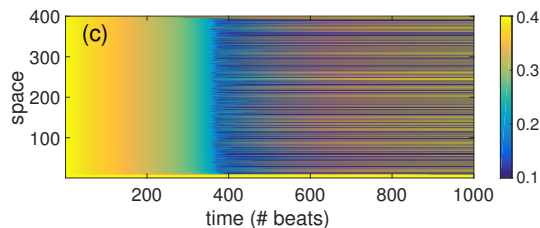
FS=1



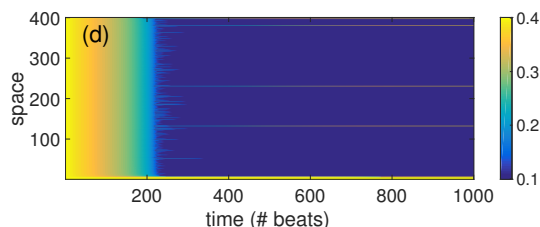
FS=1.44



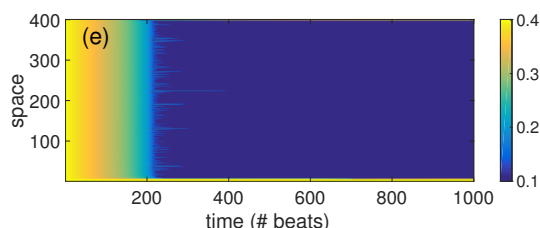
FS=1.9



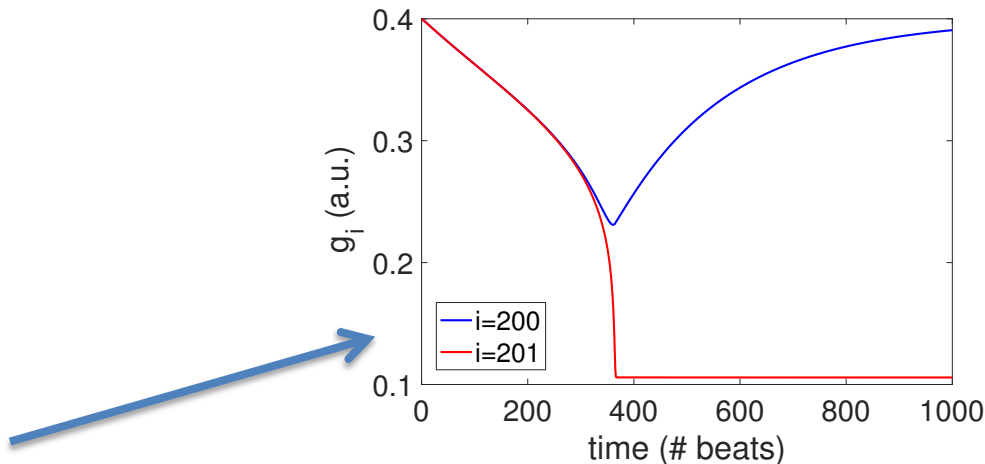
FS=3.5



FS=20

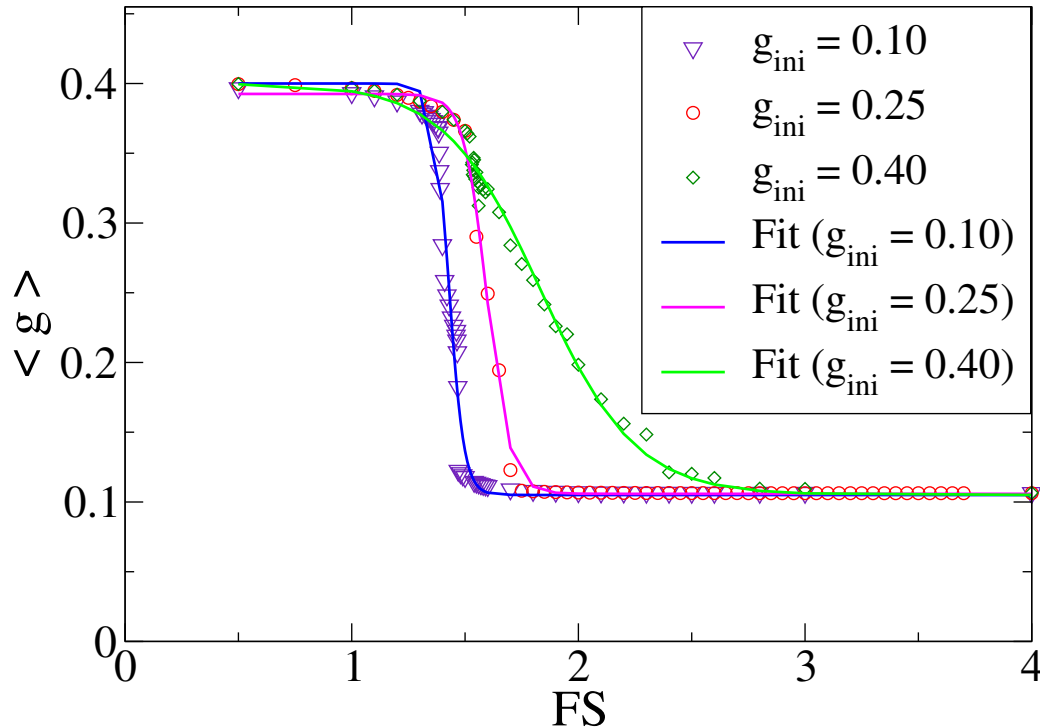


FS=1.9



We observe a transition by increasing FS from GJ conductance close to 0.4 (upper state) to GJ conductance close to 0.1 (lower state). For intermediate values of FS, we observe a spatially mixed state.

Study of the transition from UP to LOW GJ conductances

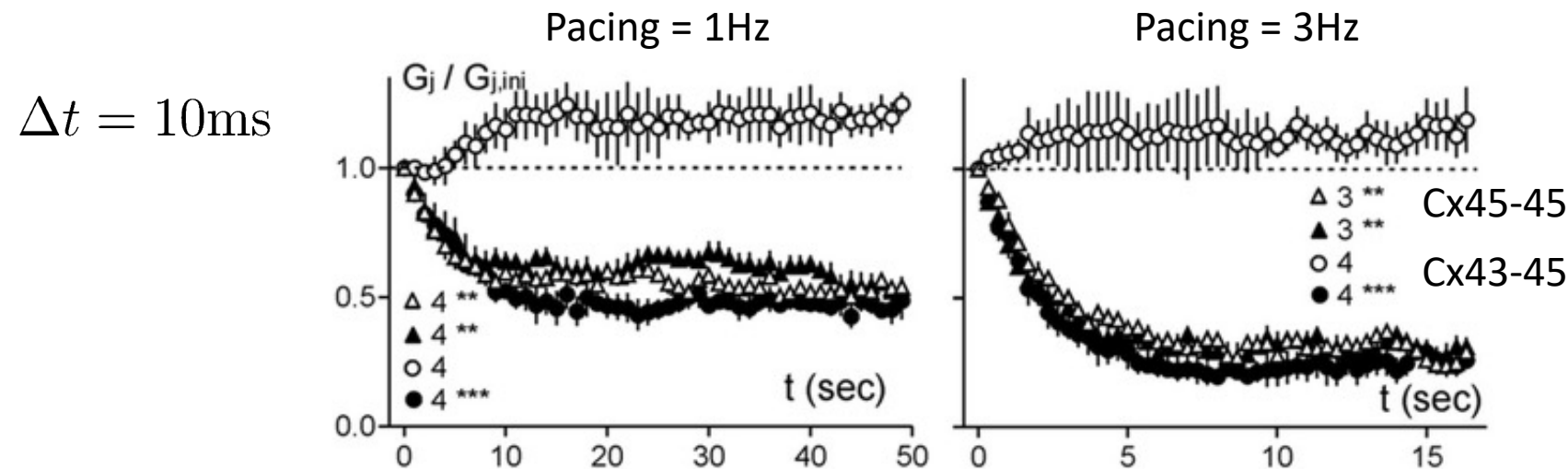


We have studied the influence of both FS and g_{ini} for characterizing the transition between upper and lower states of conductance. The spatial average of the conductance $\langle g \rangle$ is used as an **order parameter** to characterize this transition.

Related experimental study showing bistability for GJ

Junctional delay, frequency, and direction-dependent uncoupling of human heterotypic Cx45/Cx43 gap junction channels

Willy G. Ye ^{a,1}, Benny Yue ^{a,1}, Hiroshi Aoyama ^b, Nicholas K. Kim ^a, John A. Cameron ^a,
Honghong Chen ^a, Donglin Bai ^{a,*}



By varying the junctional delay Δt and the pacing frequency, they observe a different dynamics for the GJ conductances. It is also highly dependent on the GJ composition.

Acknowledgements

Collaborators:

UNAV-CIMA-CUN (Dr. Javier Diez, MD, Dr. I. Garcia-Bolao, MD, ...)

UPC Barcelona (B. Echebarria, A. Peñaranda,
I.R. Cantalapiedra, E. Alvarez-Lacalle)

Liege University (P.C. Dauby, A. Collet, ...)

Utah CVRTI (F.B. Sachse, A.C. Sankaranikutty, ...)

Max Planck Göttingen (A. Witt, S. Luther,...)

UNAV_Farma: Prof. I.F. Troconiz

Madrid_Ophtalmo. : Dr. M. Ibarz

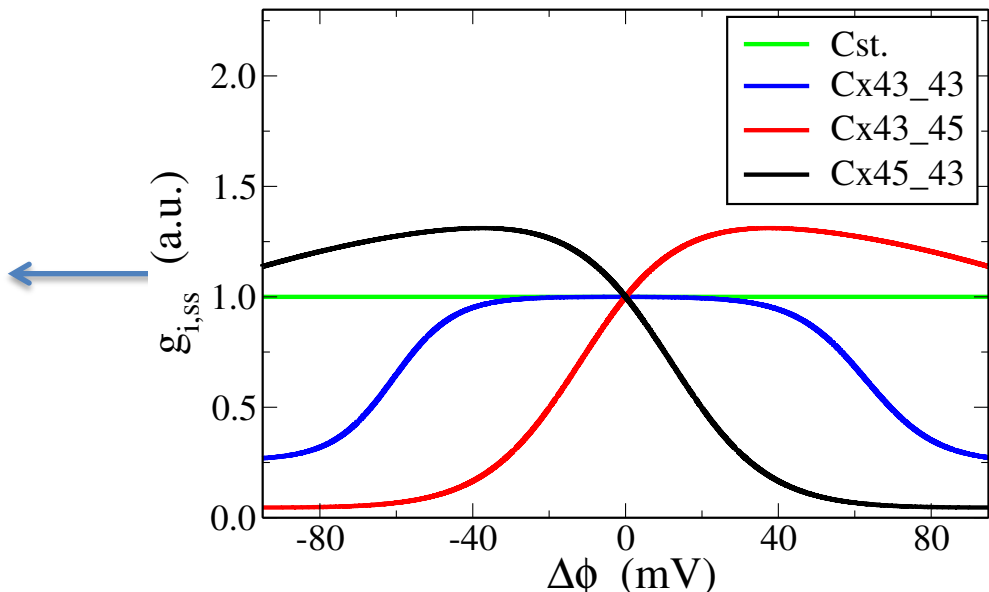
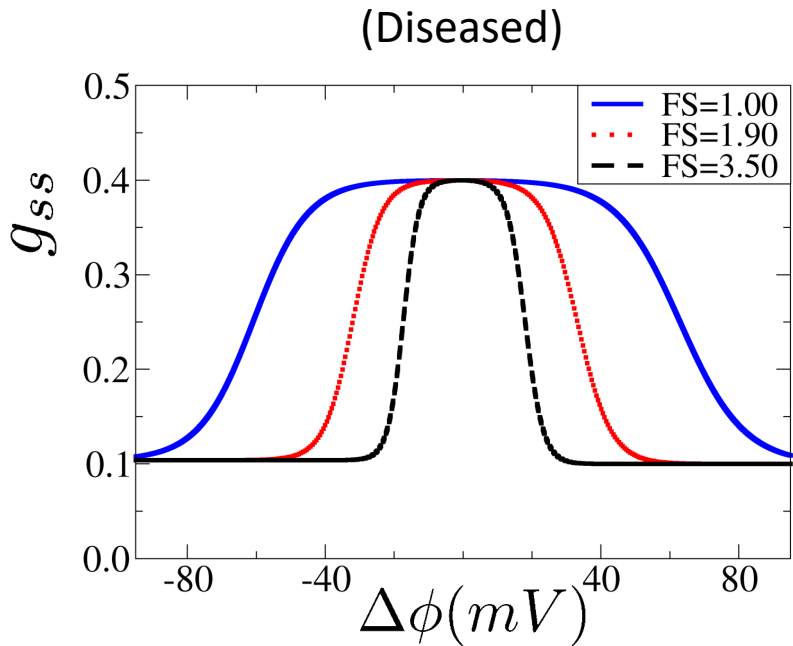
Financial support : (MINECO) under grant number PID2020-116927RB-C22
(Spain research grant)

Thank you !

1997 Summer School & Workshop/Curso de verano, Gulbenkian International Advanced. Course
INTRODUCTION TO DYNAMICAL SYSTEMS: THEORY FOR BIOSCIENCE.



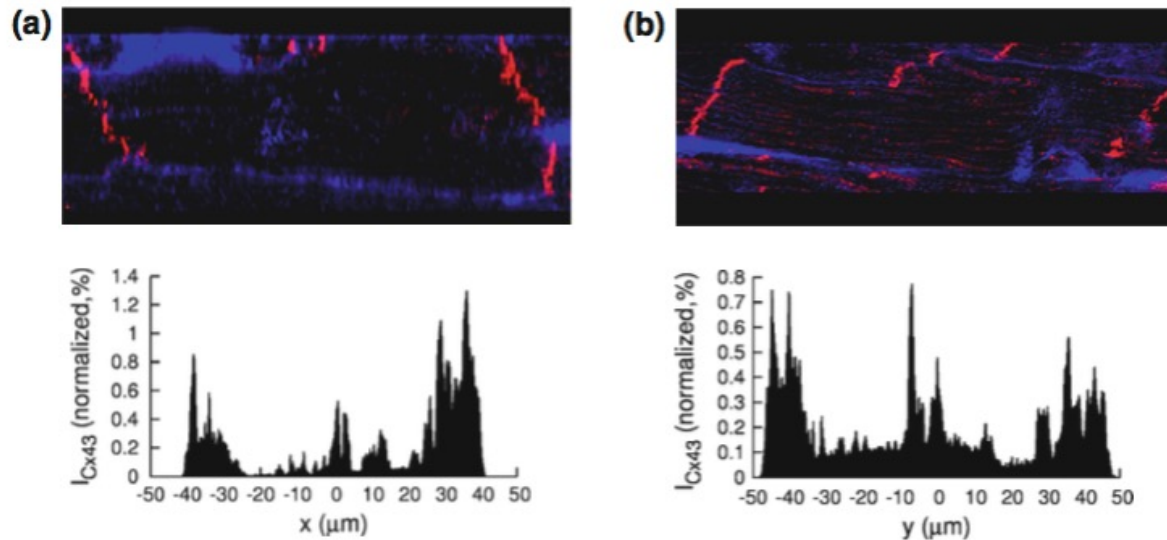
Justification of the FS factor



Heterotypic GJs have asymmetrical g_{ss} functions.

A mix of several type of GJ types may justify the FS parameter

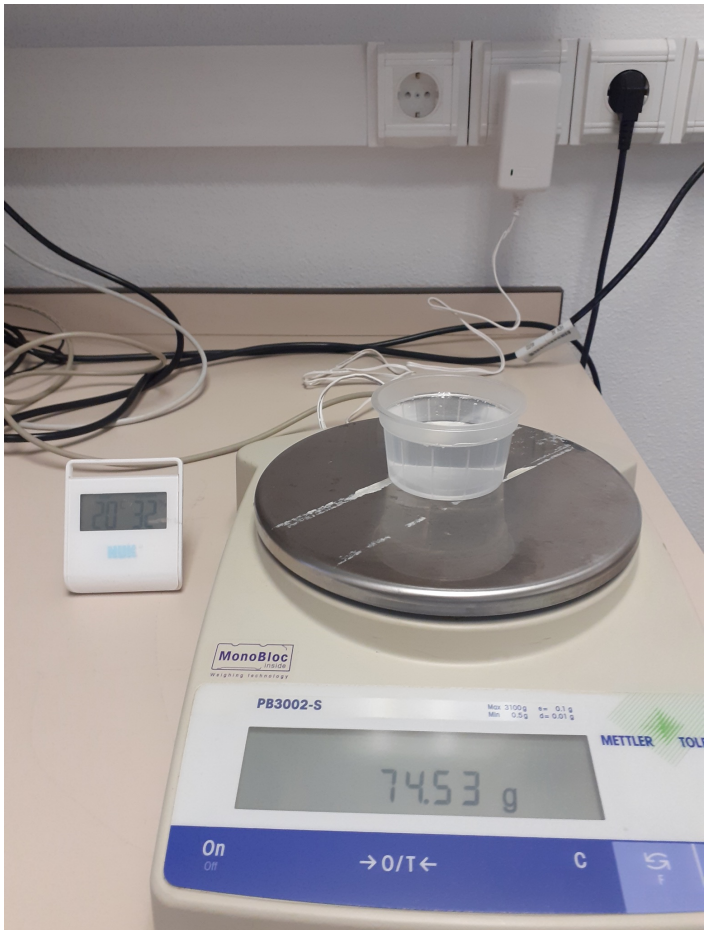
Justification of the introduction of noise (Ns)



Spatial heterogeneities and different geometric orientation
lead to variability in the GJ conductance
This may justify the noise factor

Supplementary materials (part i)

Evaporation

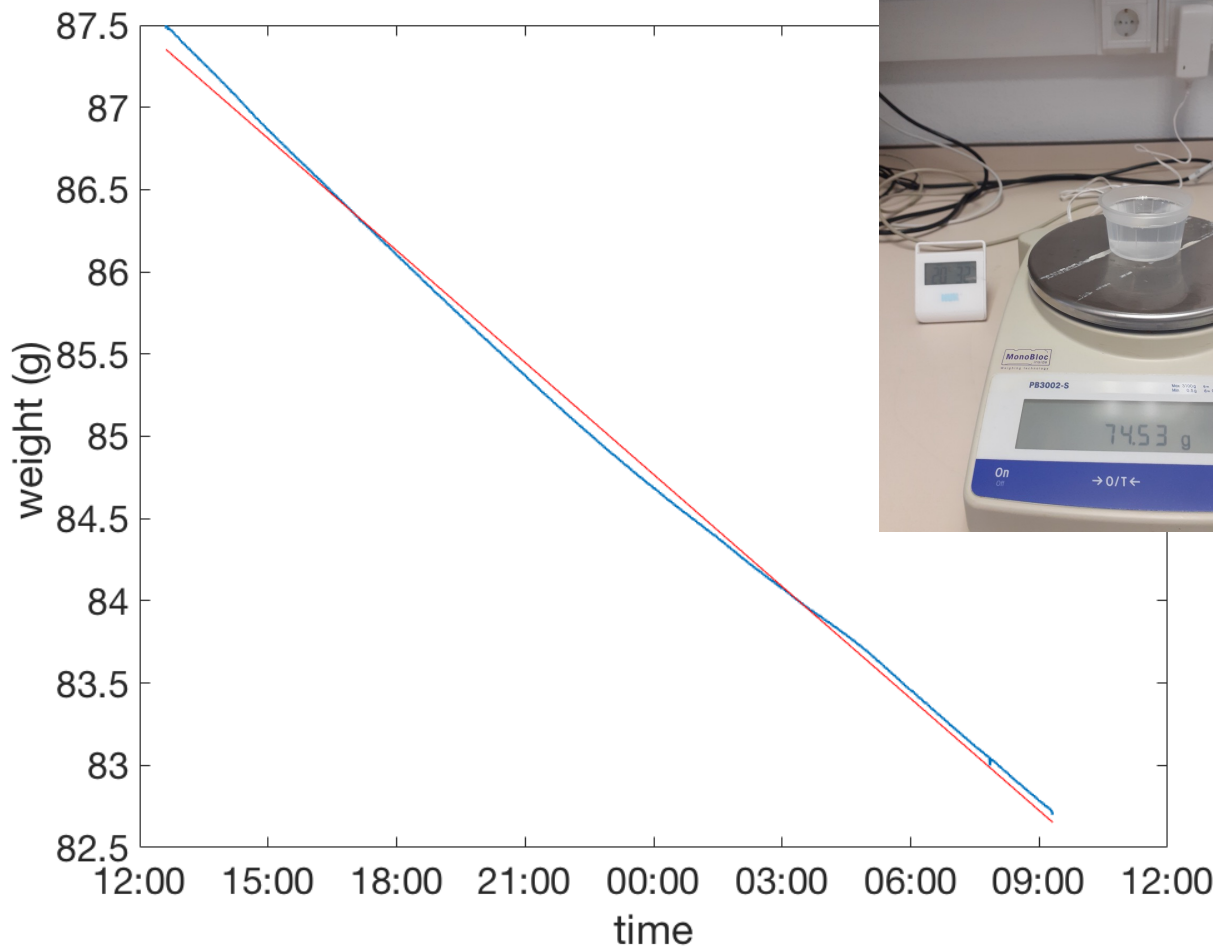


El recipiente abierto al ambiente exterior se va a vaciar (poco) debido a la evaporación del agua.

Con la balanza podemos estimar la tasa de evaporación.

$T \approx 20 \text{ }^{\circ}\text{C}$, humedad in [32-37]%

Evaporation (I)

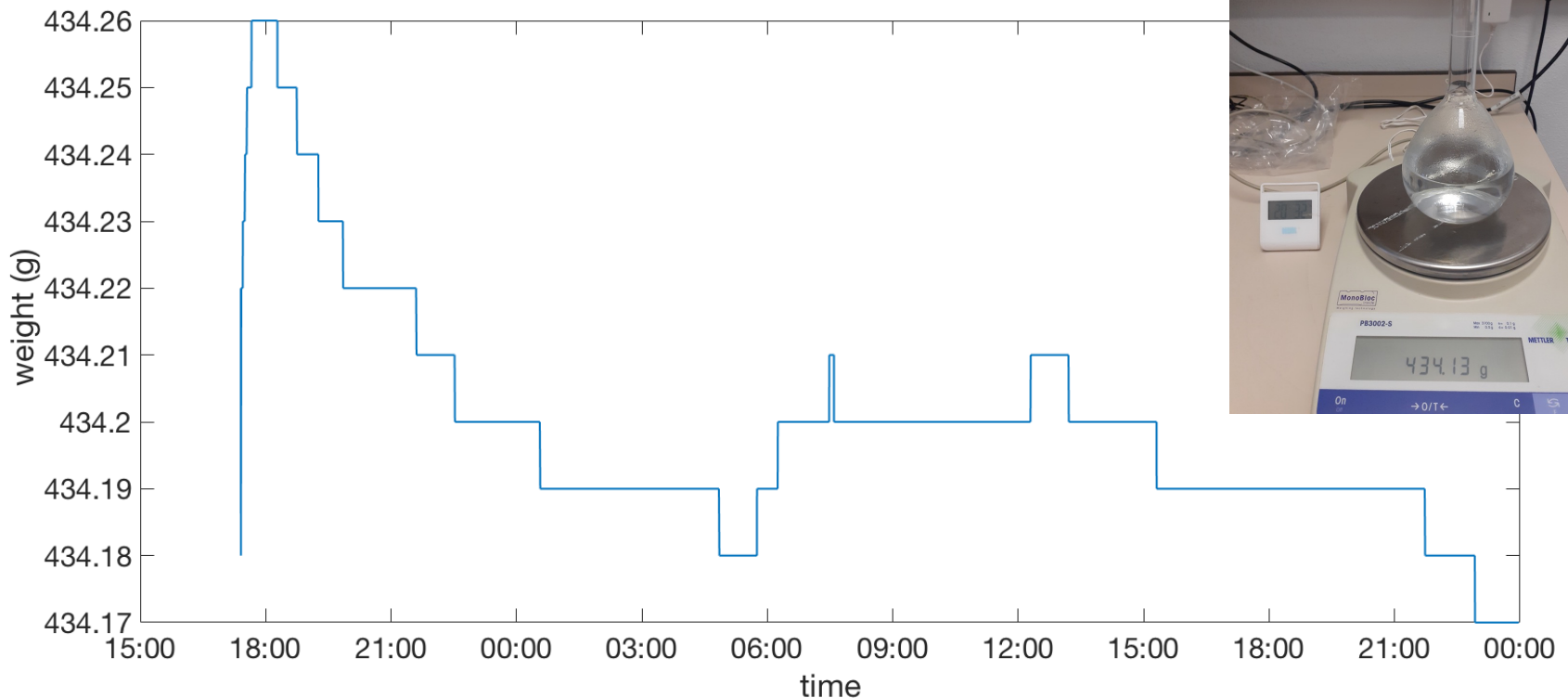


Evaporación total : -5.448 g/(24h)

Evaporación: -0.1864 g/(24h cm²)

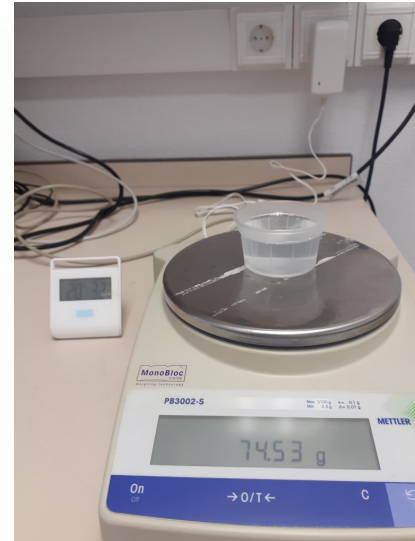
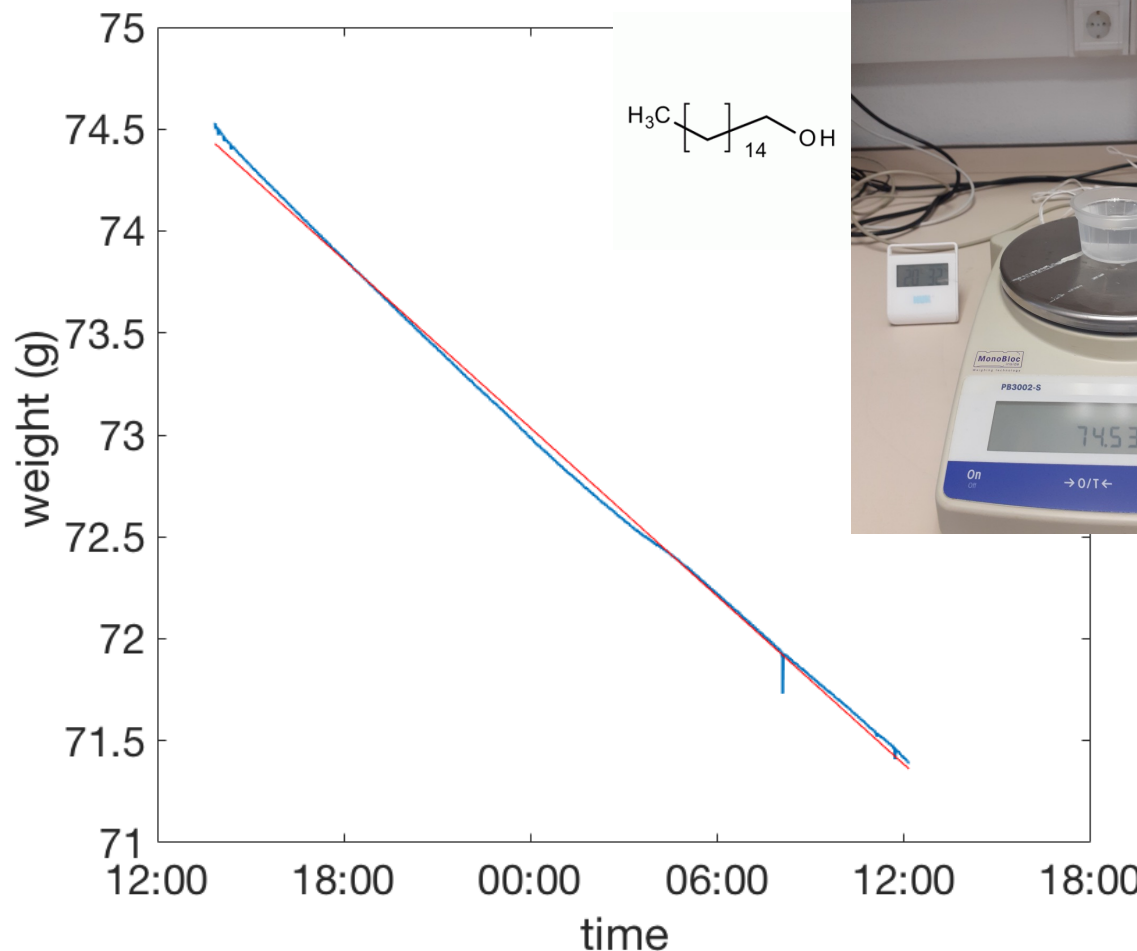
$$D = 6.1 \text{ cm}$$
$$A = 29.2 \text{ cm}^2$$

Evaporation (II)



Con el “matras” la evaporación es despreciable !

Evaporation (III)

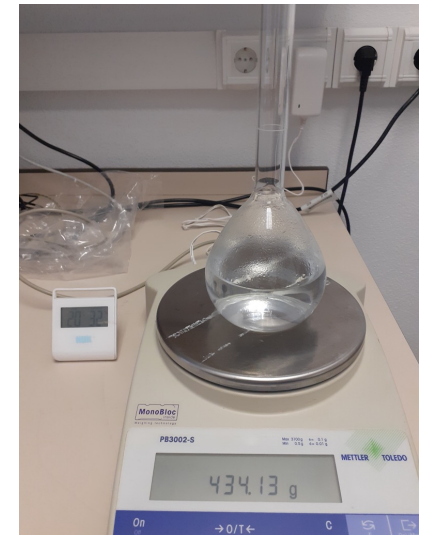
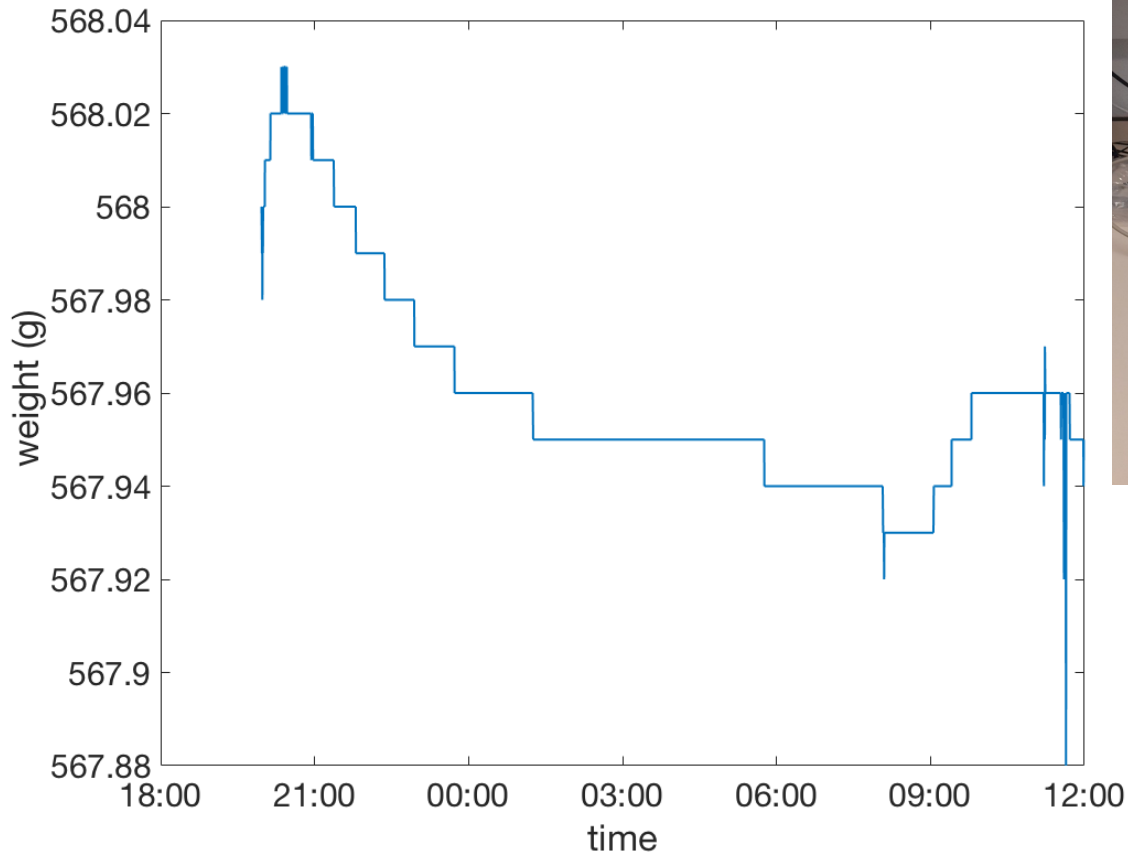


$D = 6.1 \text{ cm}$
 $A = 29.2 \text{ cm}^2$

Evaporación total : -3.301 g/(24h)

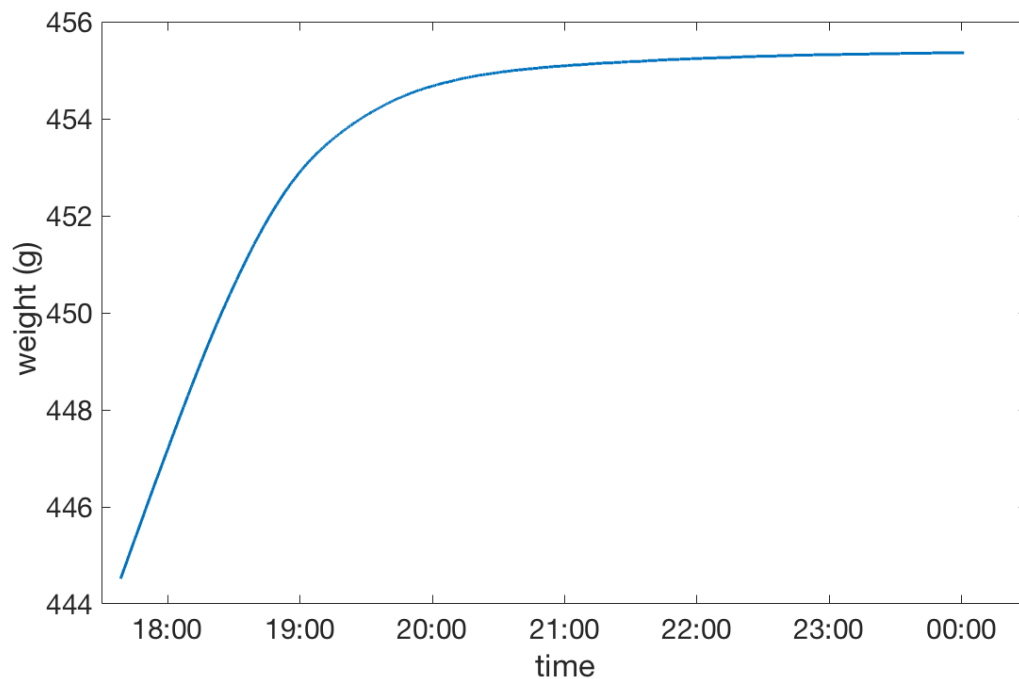
Evaporación: -0.1129 g/(24h cm²)

Evaporation (IV)



Con el “matras” grande la evaporación es también despreciable !

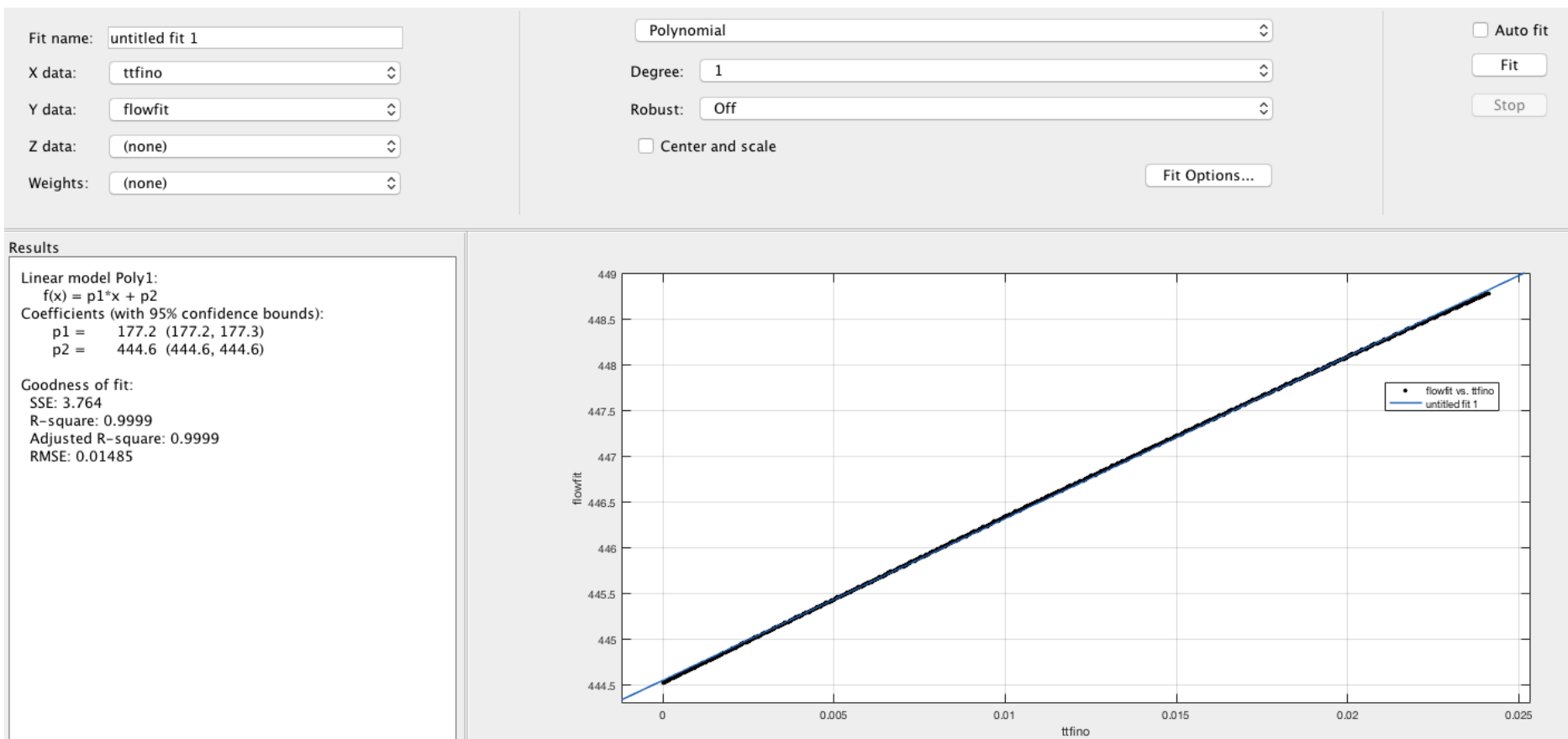
Poiseuille flow (I)



Problem : Las burbujas vienen a “disturbar ” el flujo !

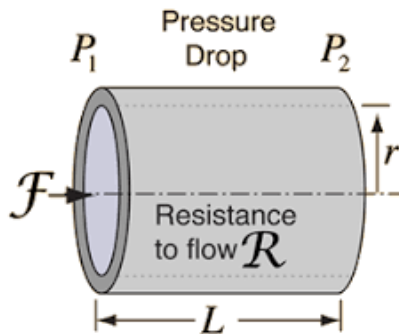
Diferencia de alturas entre la superficie superior e inferior: 129.2 cm
Peso inicial: 444.6 g , temperatura = 20ºC; humedad relativa: 37%.

Poiseuille flow (II)



Parte lineal da un crecimiento de 177.2 g/(24h) (medido sobre los 30 primeros minutos). Comprobar....

Poiseuille flow (III)



$$Q = \frac{\pi r^4 \Delta p}{8\mu L}$$

$$\Delta p = p_1 - p_2 \approx 12670.2 \text{ Pa}$$

$$L \approx 13 \text{ mm}$$

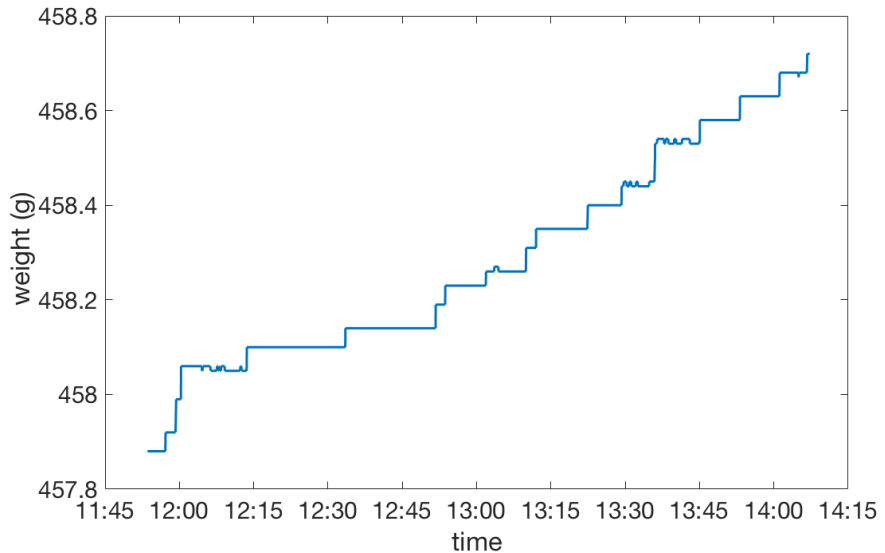
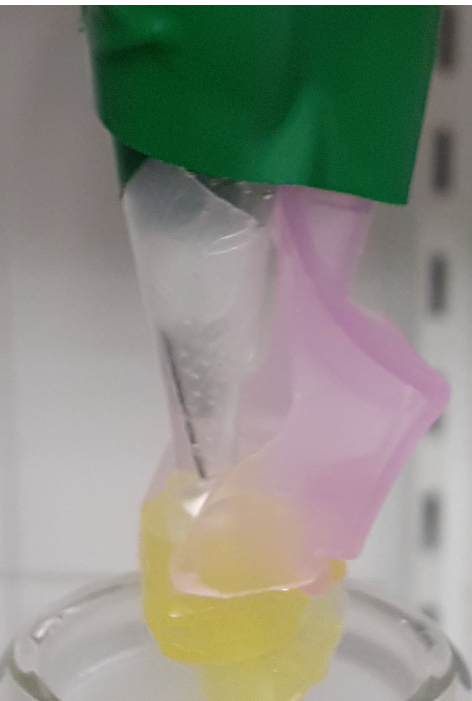
$$r \approx 0.08 \text{ mm}$$

$$\mu \approx 0.001 \text{ Pa s}$$

$$Q_{\text{exper.}} = 2.051 \mu\text{l/s} = 177.2 \text{ g/(24h)}$$

$$Q_{\text{teor.}} = 15.677 \mu\text{l/s} = 1354.5 \text{ g/(24h)}$$

Drop experiment (I)

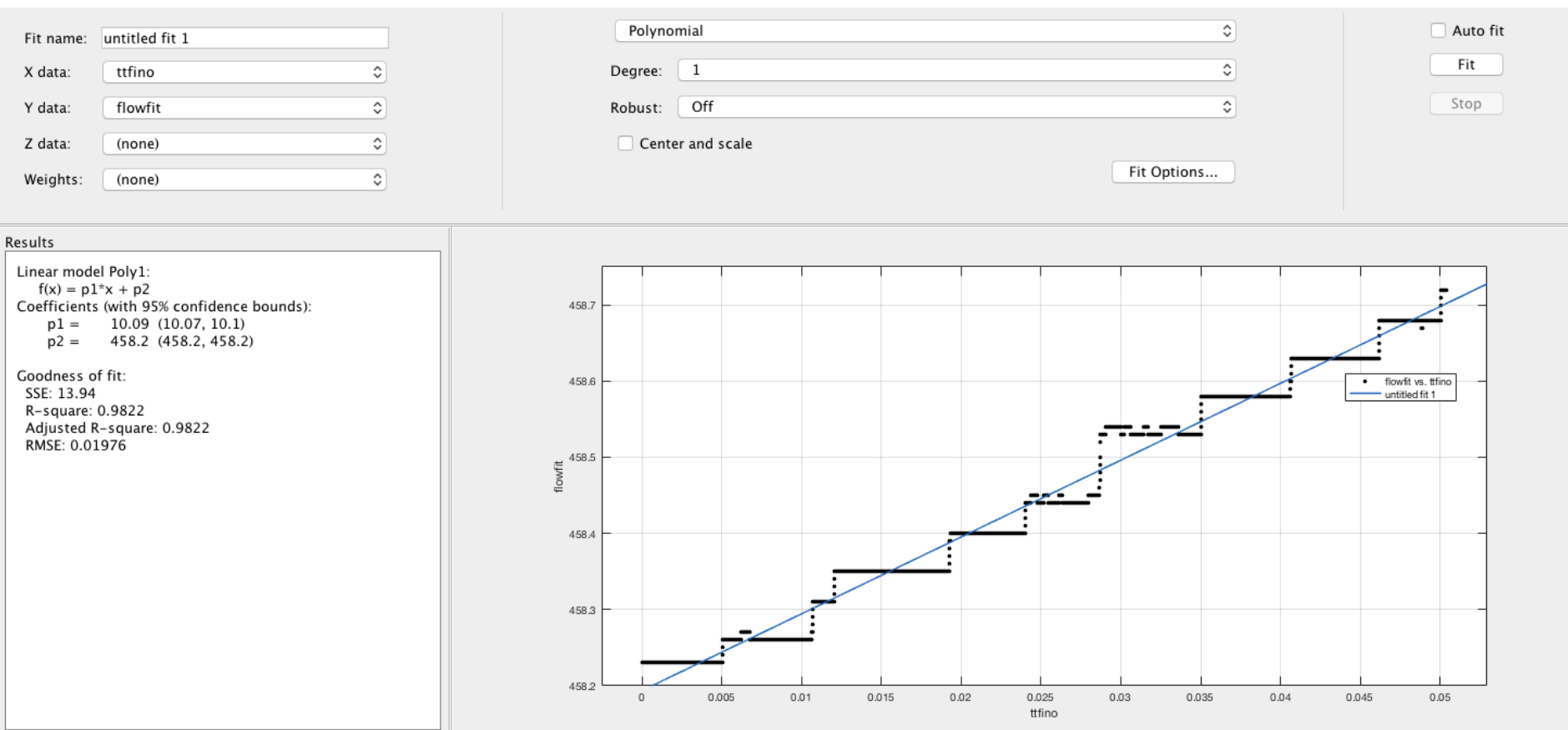


Dejamos caer las gotas desde una pipeta.

Altura de agua en la pipeta (approx.): 15 cm

Peso inicial: 457.68 g; Temperatura = 20ºC; humedad relativa: 34%.

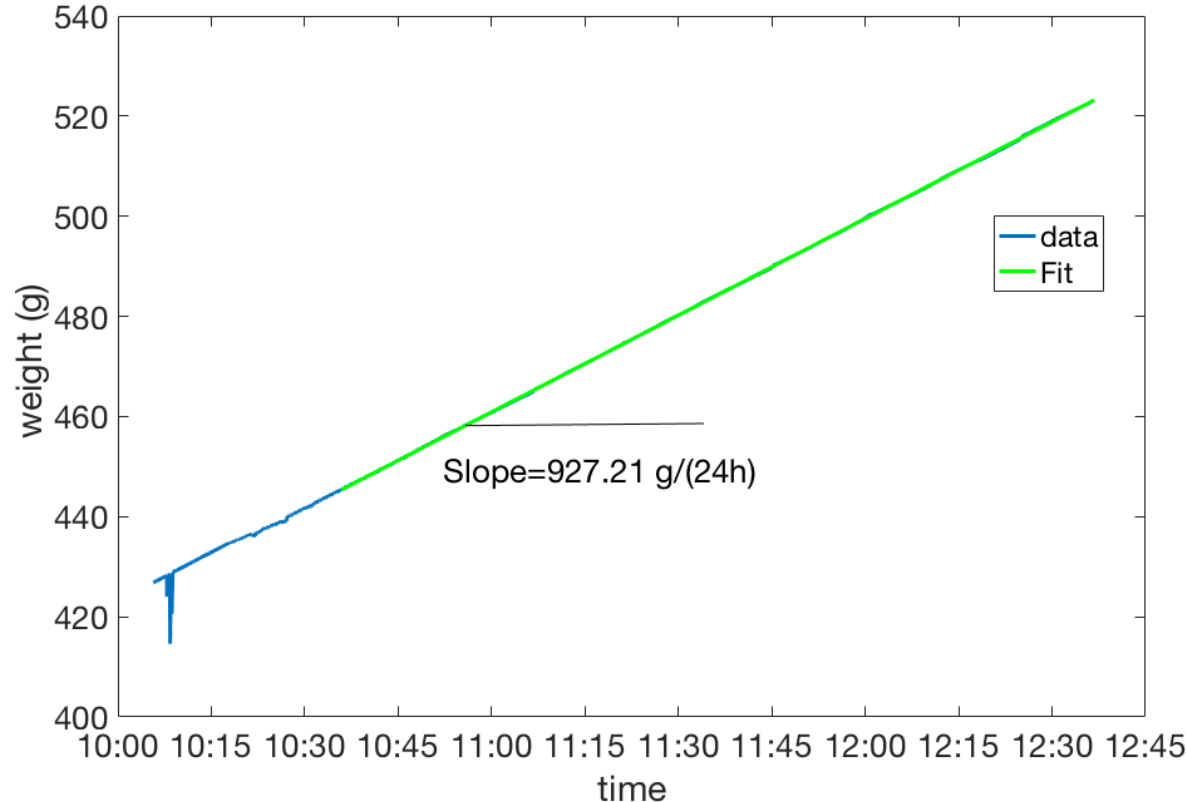
Drop experiment (II)



Parte lineal da un crecimiento de $10.1 \text{ g}/(24\text{h})$ (medido entre 12:54 y las 14:07).

Con esta altura de fluido, Poiseuille da $Q=157.2 \text{ g}/(24\text{h})$.

Poiseuille flow (March 01)



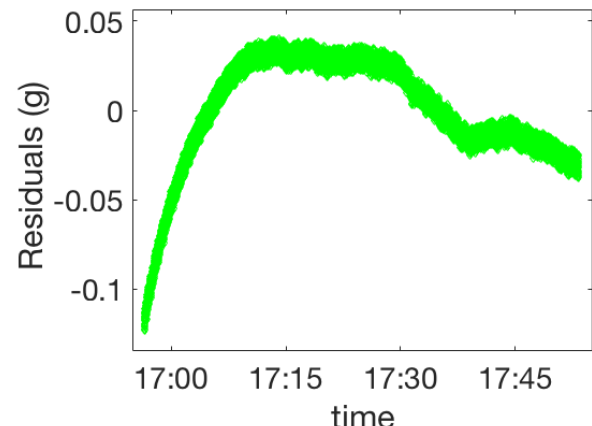
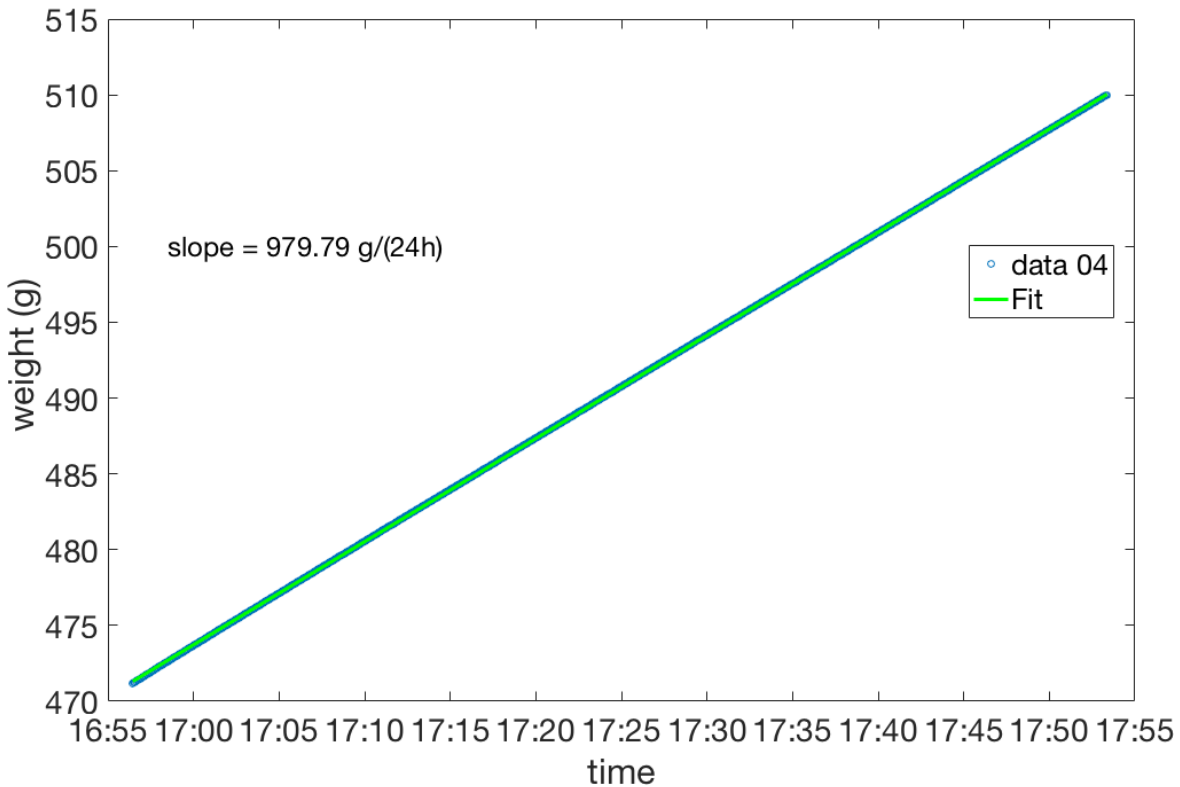
Valor calculado a partir de Poiseuille $\approx 1300 \text{ g}/(24\text{h})$

Valor medido (linear fit) $\approx 927 \text{ g}/(24\text{h})$

Diferencia de alturas entre la superficie superior e inferior (inicial) : 127.4 cm

Peso inicial: 426.84 g , temperatura = 19°C; humedad relativa: 37%.

Poiseuille flow (March 02, A)



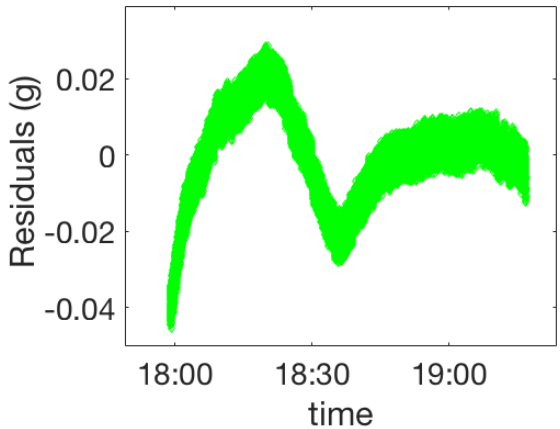
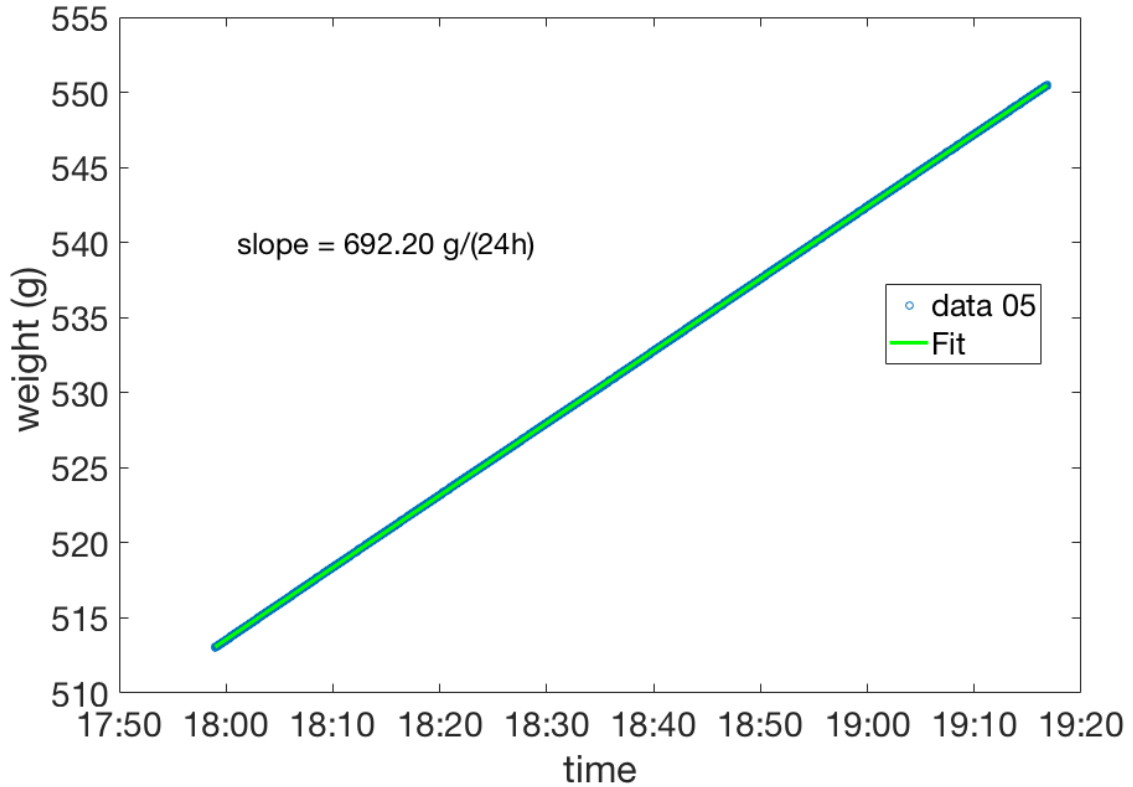
(data_file: capture_flow_04)

Valor medido (linear fit) $\approx 979.79 \text{ g}/(24\text{h})$ (CI 95%: [979.76 ; 979.83])

Diferencia de alturas entre la superficie superior e inferior (inicial) : $\Delta h=127.5 \text{ cm}$

Peso inicial: 470.75 g , temperatura = 20ºC; humedad relativa: 34%.

Poiseuille flow (March 02, B)



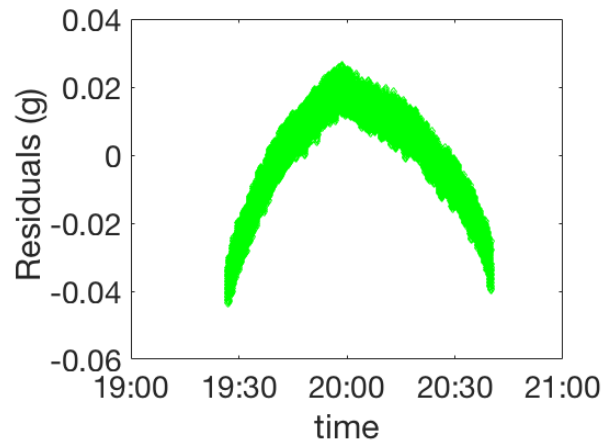
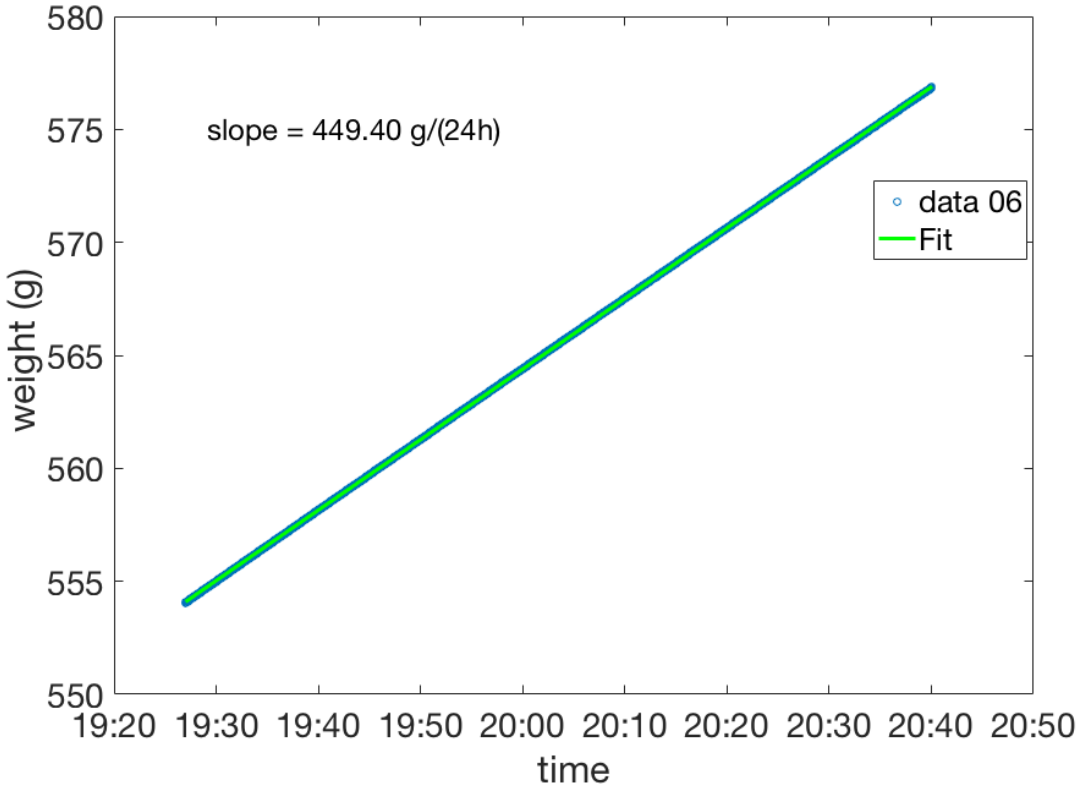
(data_file: capture_flow_05)

Valor medido (linear fit) $\approx 692.20 \text{ g}/(24\text{h})$ (CI 95%: [692.19 ; 692.21])

Diferencia de alturas entre la superficie superior e inferior (inicial) : $\Delta h = 90.5 \text{ cm}$

Peso inicial: 512.80 g , temperatura = 20°C; humedad relativa: 35%.

Poiseuille flow (March 02, C)



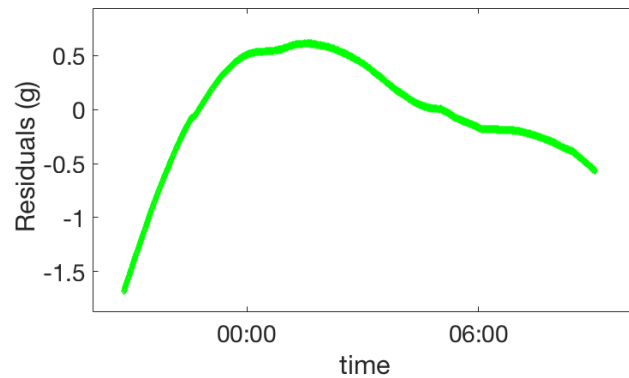
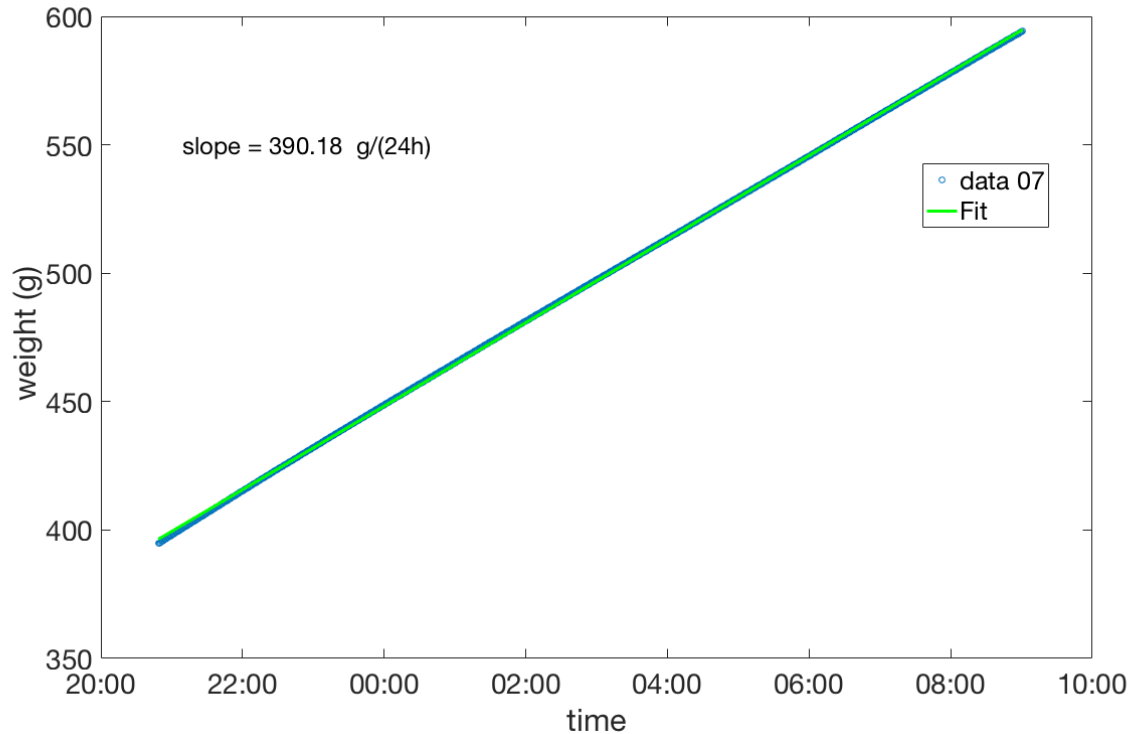
(data_file: capture_flow_06)

Valor medido (linear fit) $\approx 449.40 \text{ g}/(24\text{h})$ (CI 95%: [449.39 ; 449.41])

Diferencia de alturas entre la superficie superior e inferior (inicial) : $\Delta h = 58 \text{ cm}$

Peso inicial: 553.75 g , temperatura = 20°C; humedad relativa: 35%.

Poiseuille flow (March 02, D)



(data_file: capture_flow_07)

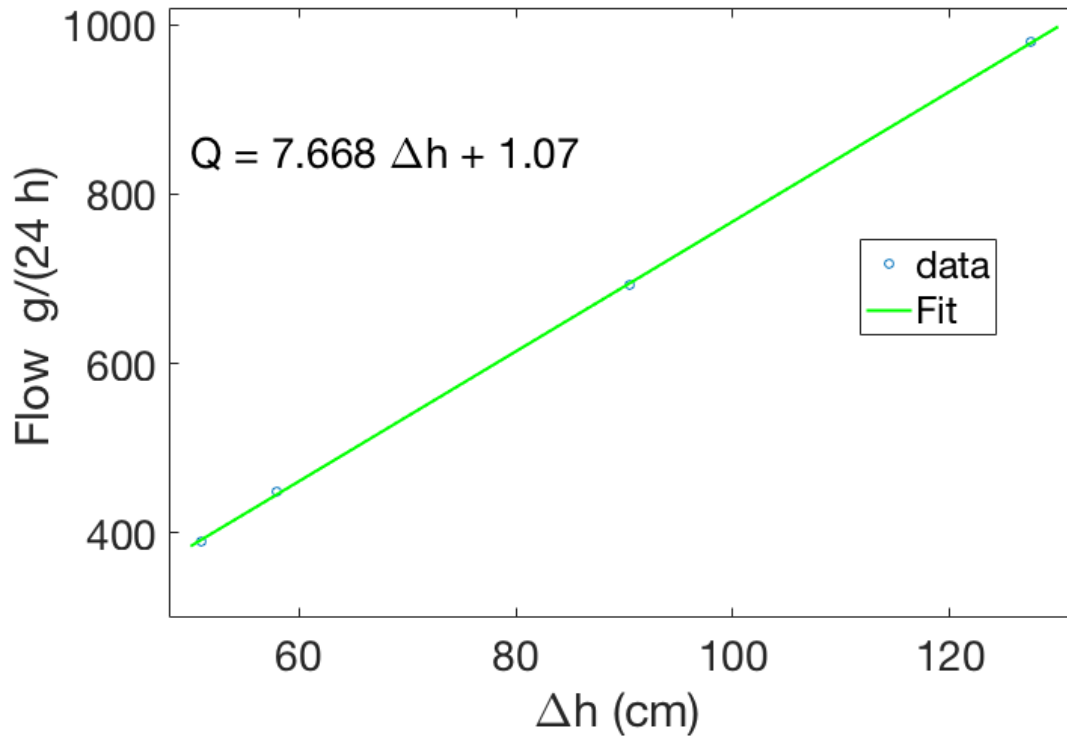
Valor medido (linear fit) $\approx 390.18 \text{ g}/(24\text{h})$ (CI 95%: [390.17 ; 390.19])

Diferencia de alturas entre la superficie superior e inferior

(inicial & final) : $\Delta h = 53 \text{ cm}$ & $\Delta h = 50.8 \text{ cm}$

Peso inicial: 394.43 g , temperatura = 20°C; humedad relativa: 34%.

Poiseuille flow (March 02, All)



Resumen:

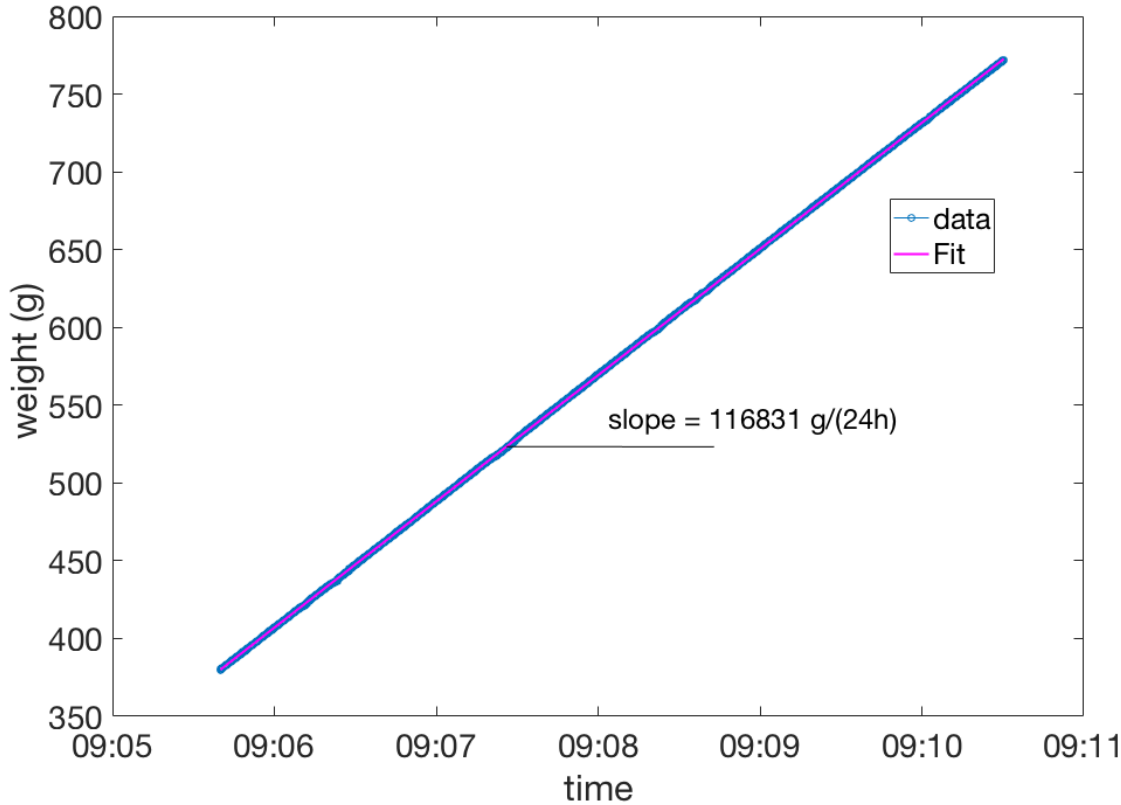
Valor medido (linear fit) $Q=7.668 \Delta h +1.07 \text{ g}/(24\text{h})$

(CIs 95%: [7.413 ; 7.922] & [-21.13 ; 23.27])

Teoría (1cm H₂O=98.0665 Pa)

Slope (teo.)=10.484 g/(24h x cm) Error: -27% !

Poiseuille flow (March 03)



Sin capsula ! Solamente la vía (longitud approx. 207.5 cm)

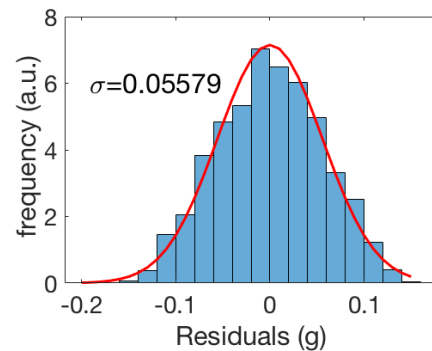
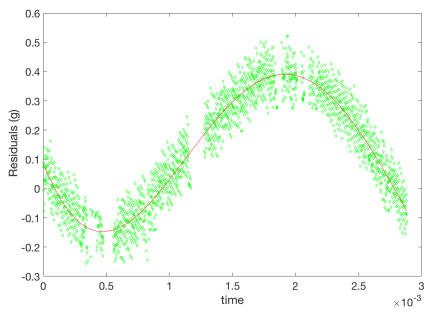
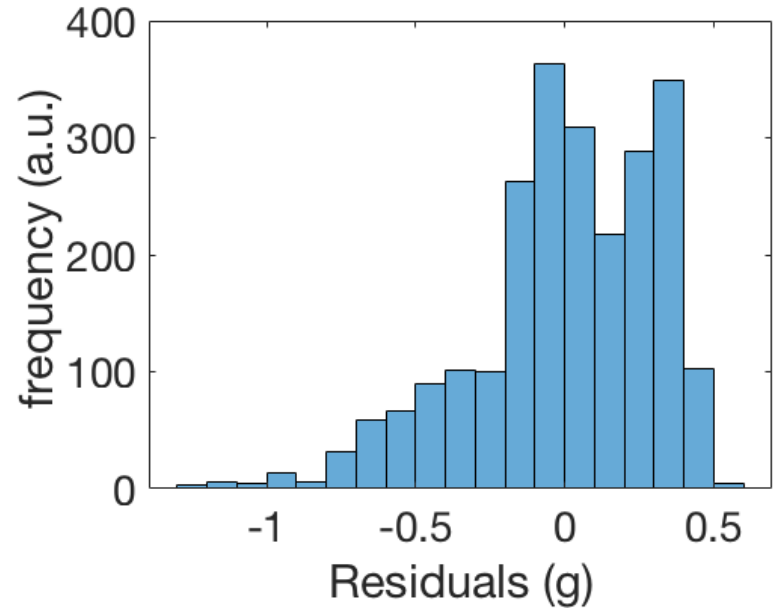
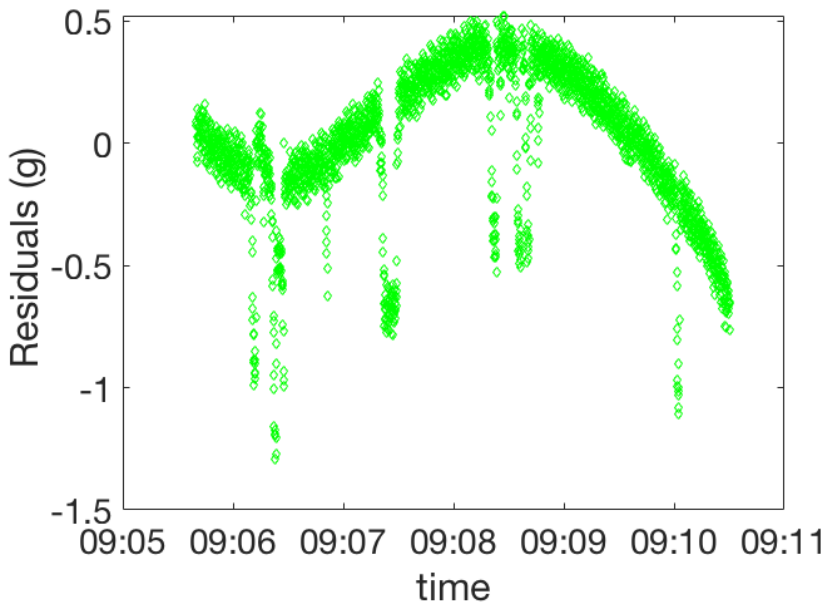
Valor medido (linear fit) $\approx 116831 \text{ g}/(24\text{h})$ CI(116818; 116844); $R^2=0.999993$

Diferencia de alturas entre la superficie superior e inferior (inicial e final) : 52.2 & 48.6 (cm)

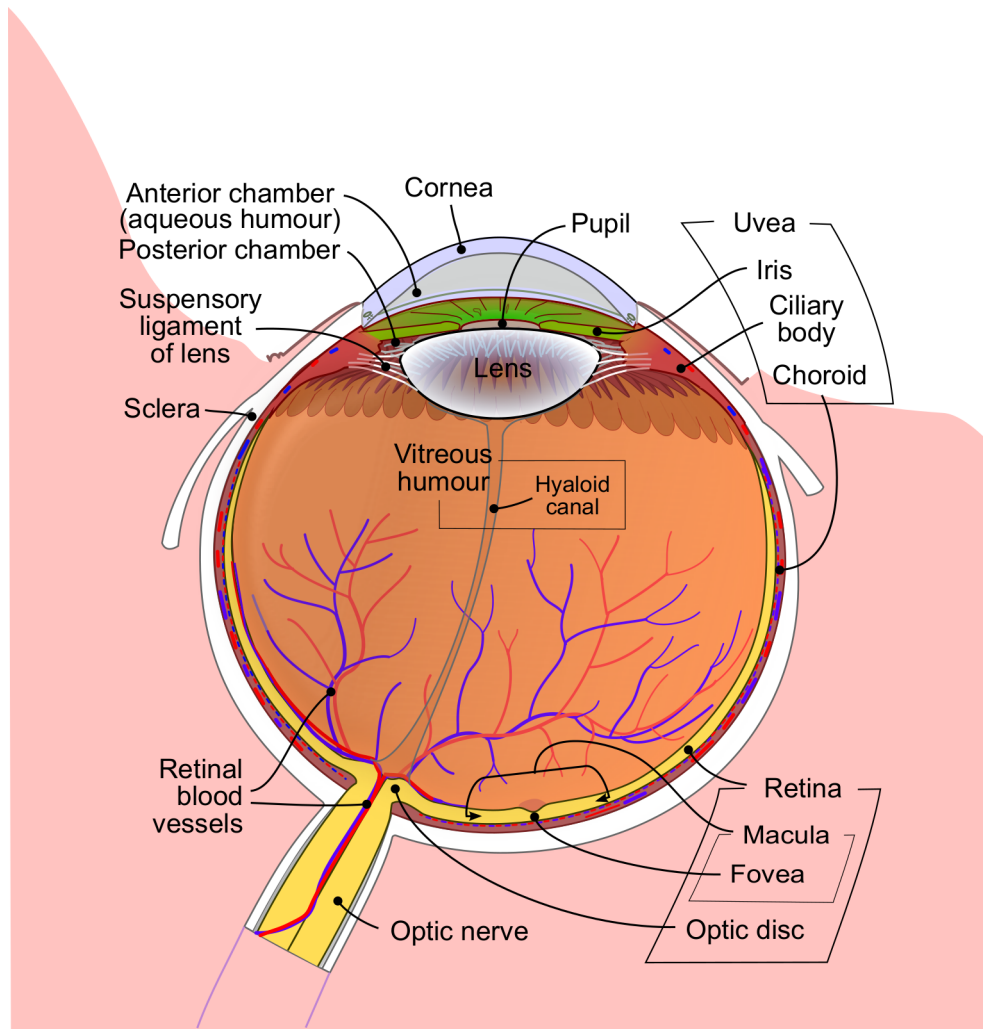
Temperatura = 20°C; humedad relativa: 34% (datos: flow_08)

Poiseuille flow (March 03)

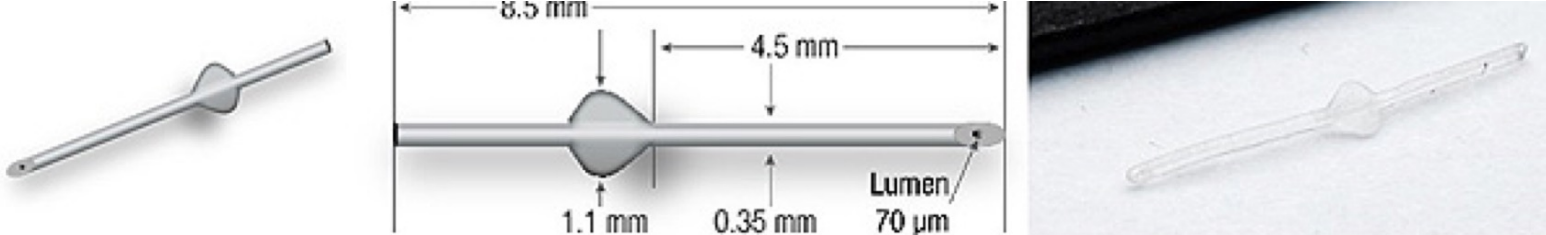
Residuals !?



Visita 16 abril 2021



Preserflo: longitud 8,5 mm, diámetro interno 70 micras



Características implante Preserflo:

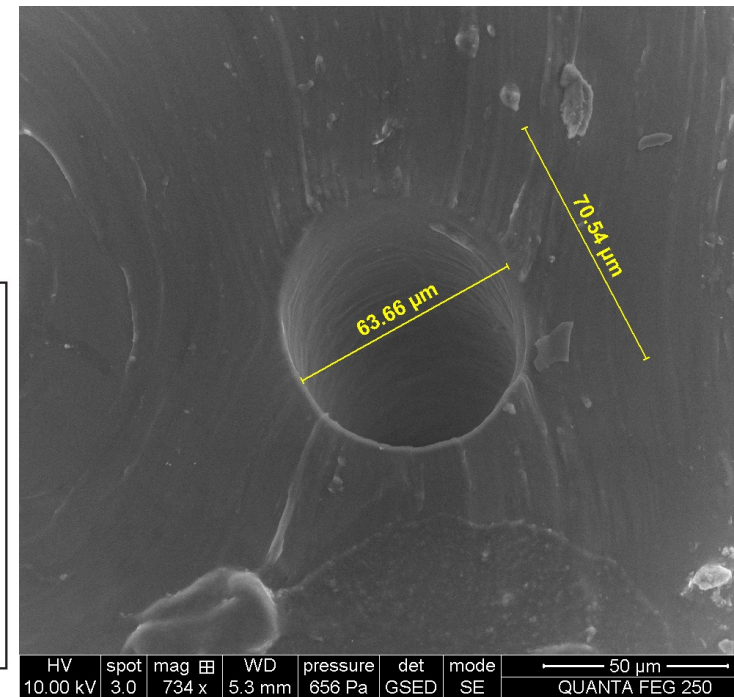
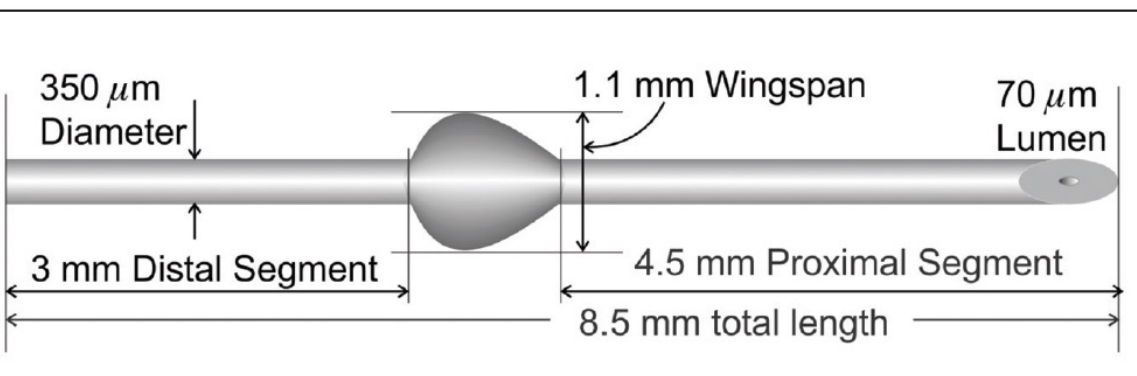
Longitud: 8,5 mm

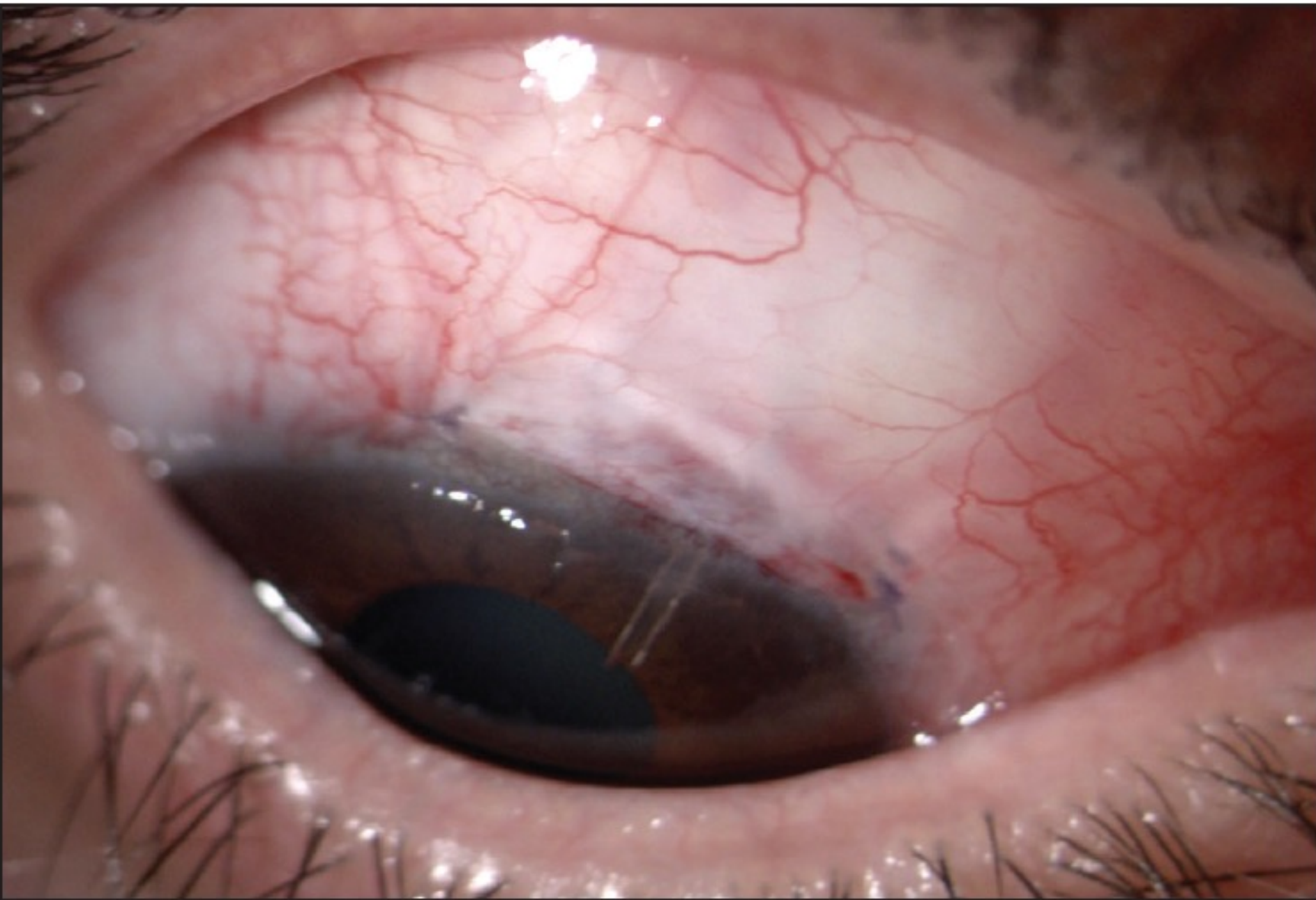
Lumen: 70 micras

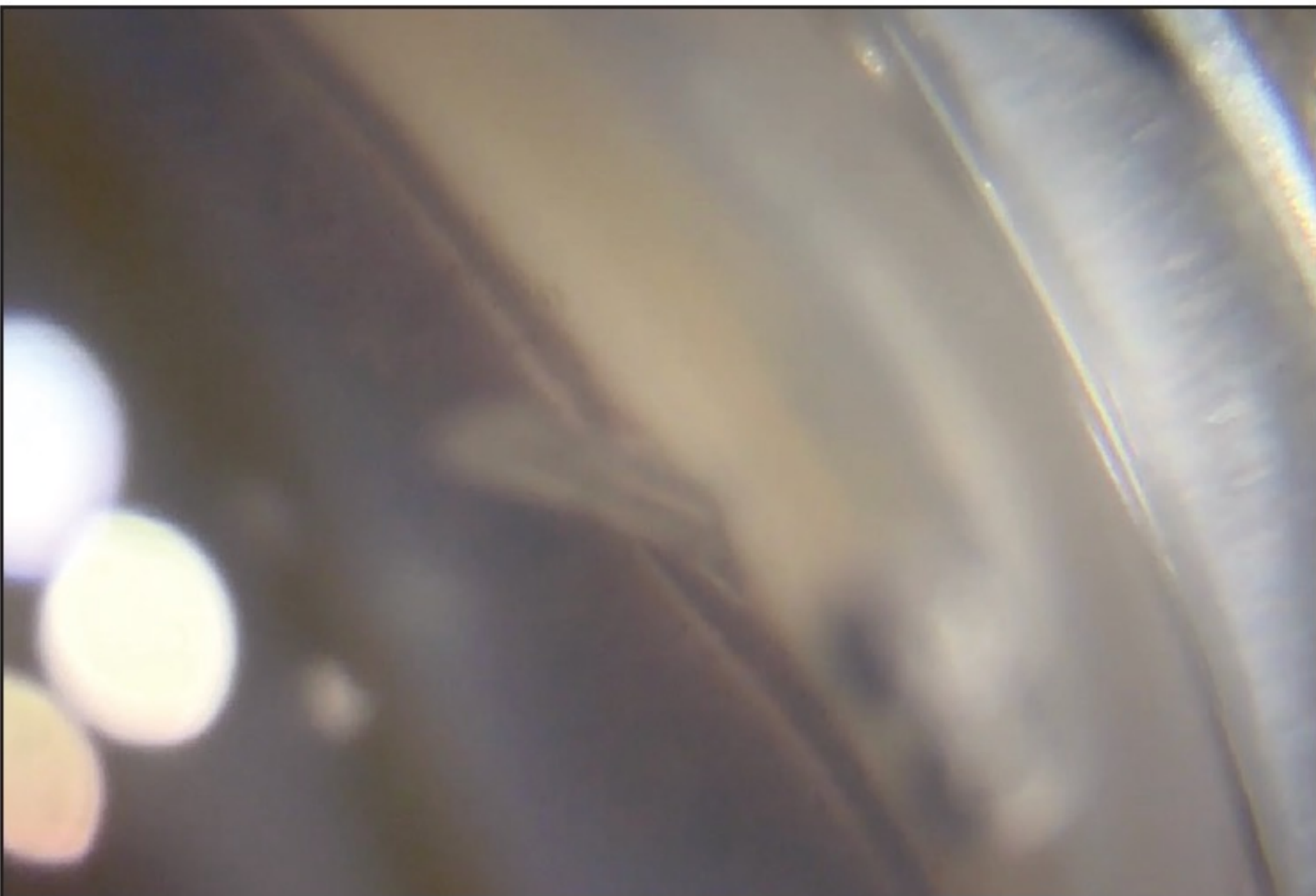
Diámetro externo: 350 micras.

Resistencia al flujo: $R = 1,30 \text{ (mmHg}/(\mu\text{L/min})$

Flujo de humor acuoso: 2 microL/min

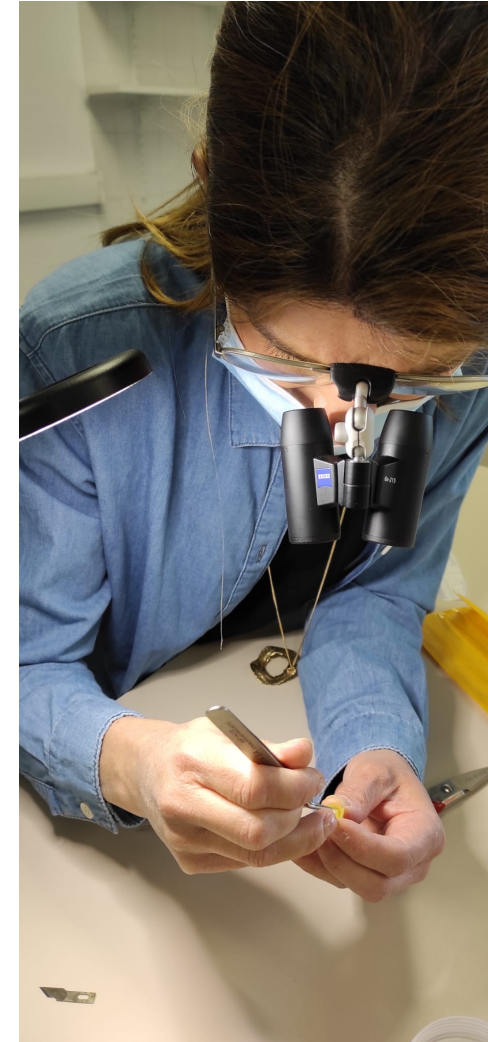
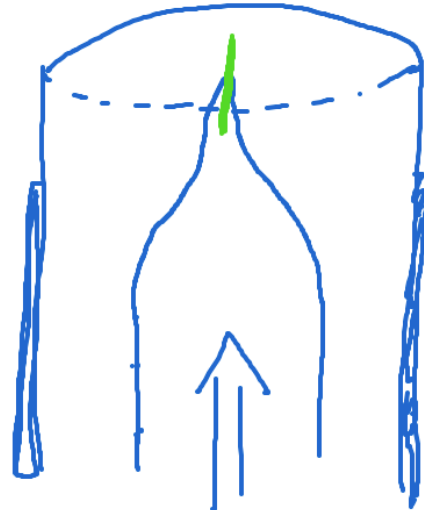






<https://www.hopkinsmedicine.org/wilmer/services/glaucoma/book/ch17s01.html>

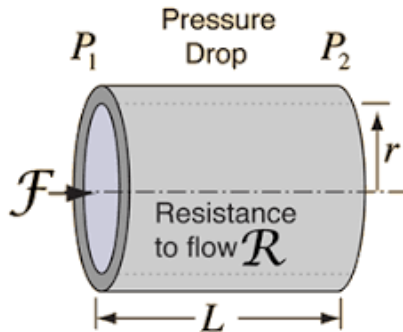
Preserflo: longitud 8,5 mm, diámetro interno 70 micras



26 abril 2021



Poiseuille flow (IV)



$$Q = \frac{\pi r^4 \Delta p}{8\mu L}$$

$$\Delta p = p_1 - p_2 \approx 20000 \text{ Pa}$$

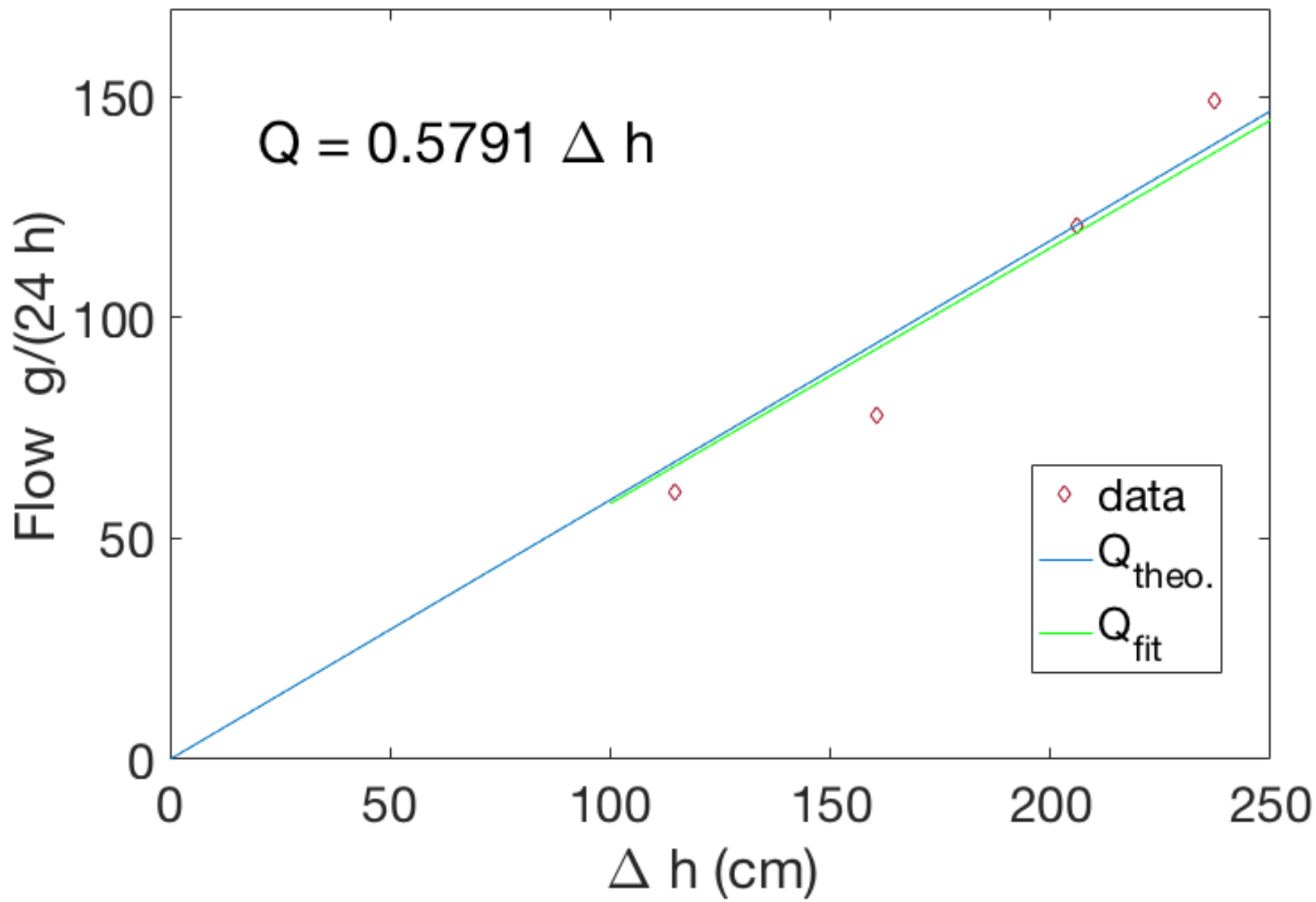
$$L \approx 8.5 \text{ mm}$$

$$r \approx 0.035 \text{ mm}$$

$$\mu \approx 0.001 \text{ Pa s}$$

$$Q_{\text{teor.}} = 1.3866 \mu\text{l/s} = 119.8 \text{ g/(24h)}$$

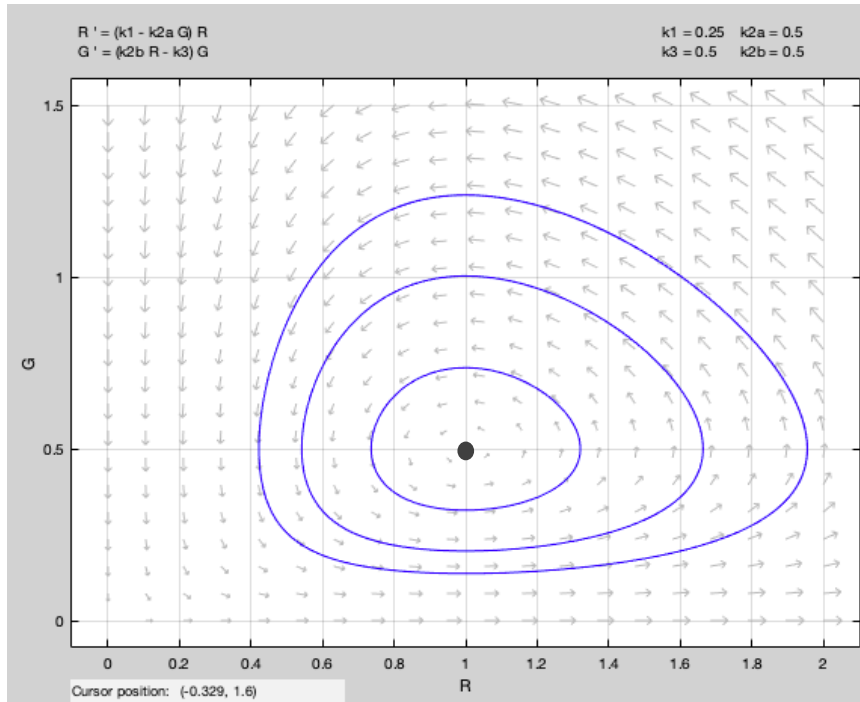
$$Q_{\text{exper.}} = 2.051 \mu\text{l/s} = 177.2 \text{ g/(24h)}$$



Supplementary materials (part ii)

Depredador-presa

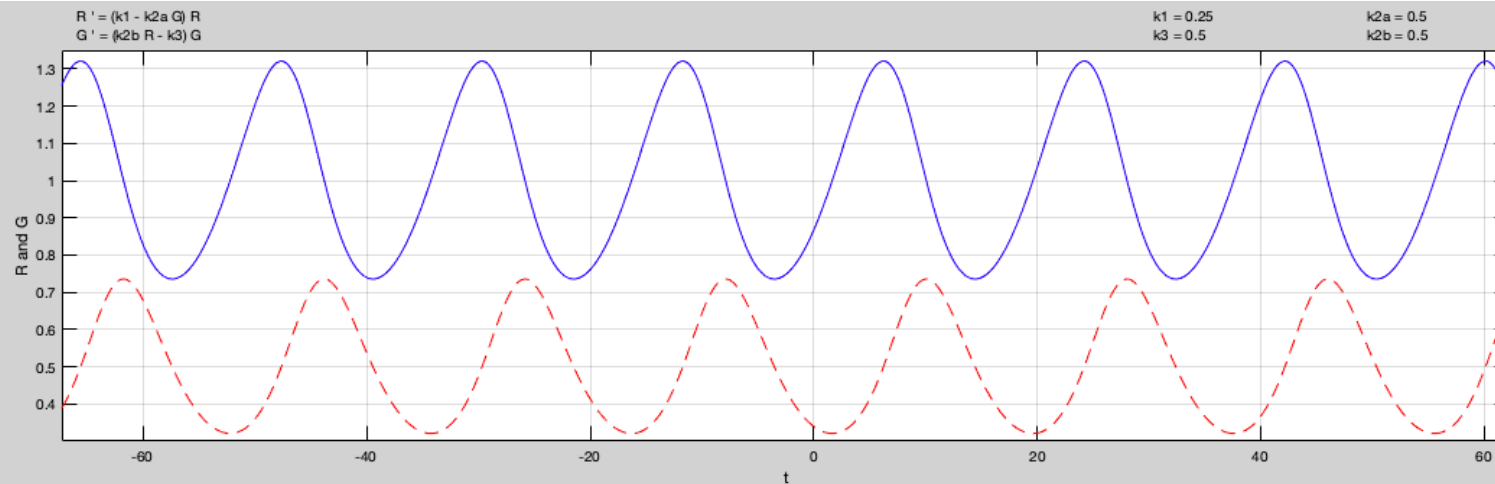
Depredador (G) – presa (R)



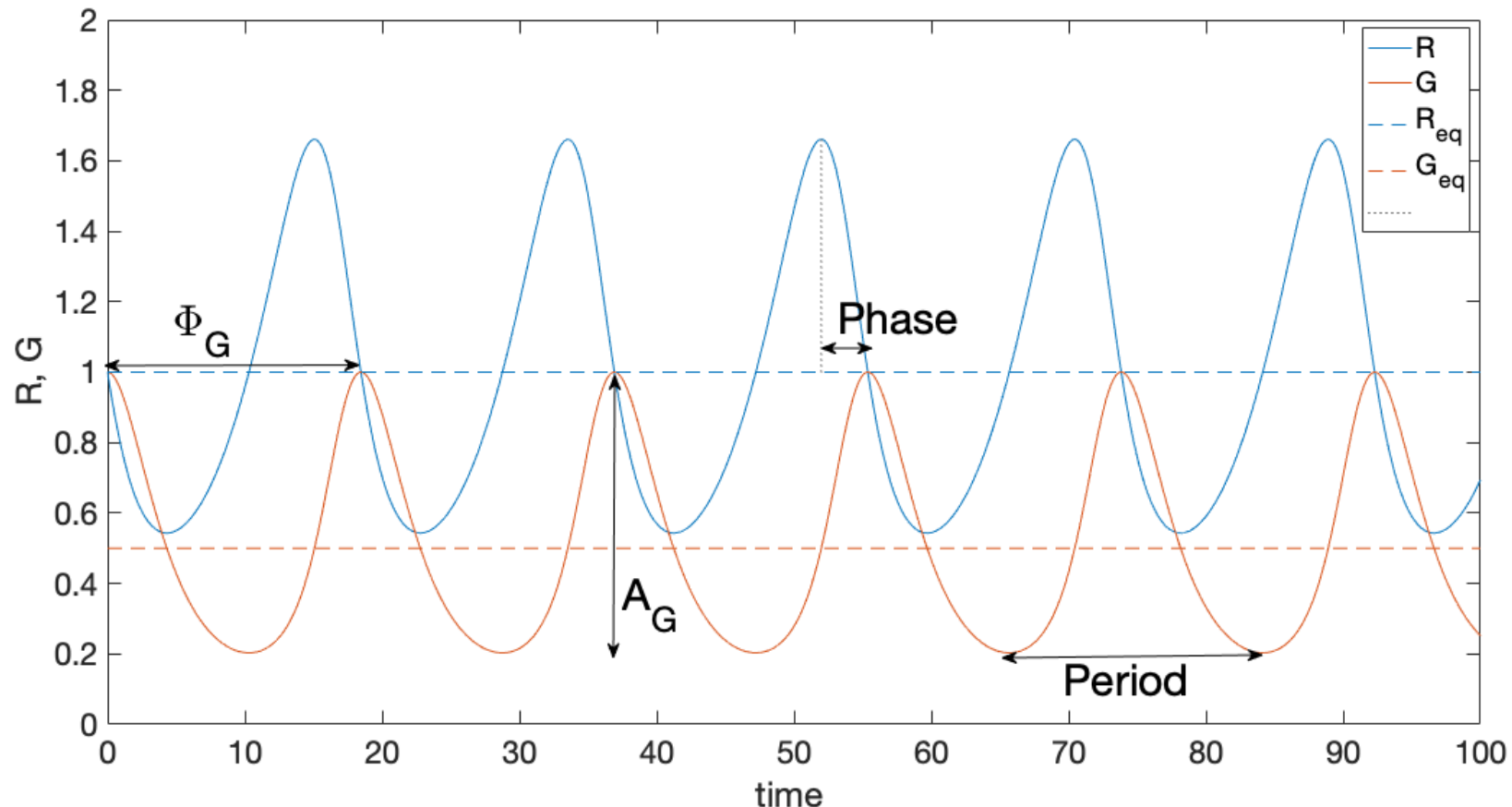
$$\frac{dR}{dt} = k_1 R - k_2 R G$$

$$\frac{dG}{dt} = k_2 R G - k_3 G$$

$$G_{eq} = \frac{k_1}{k_2} \quad R_{eq} = \frac{k_3}{k_2}$$



Ejemplo 1, Dep. (G) –presa (R)

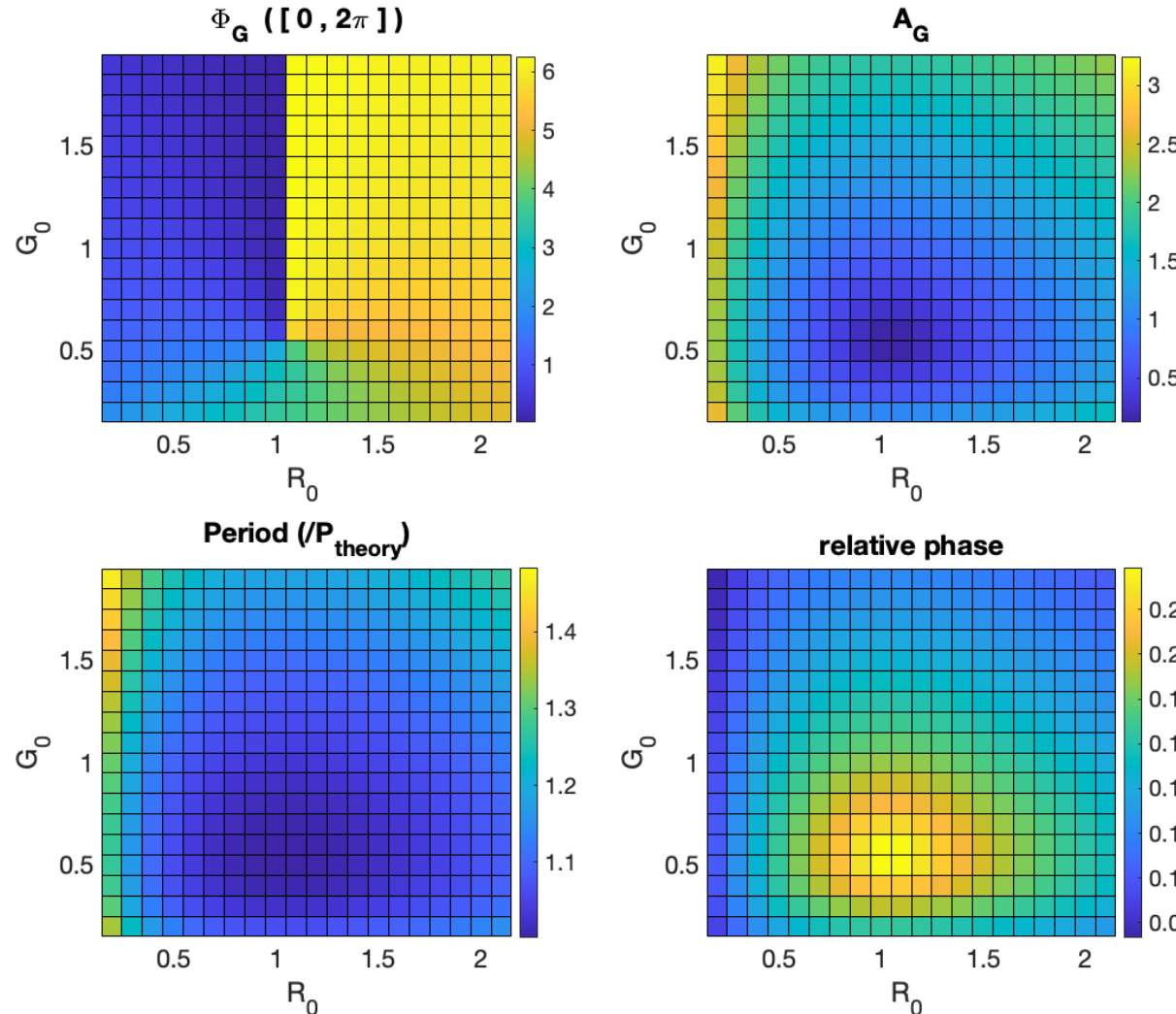


Here we have set the initial conditions: $G_0 = 1$ $R_0 = 1$

After, we will look at the influence of the initial conditions.

$$k_1 = 0.25; k_2 = 0.5; k_3 = 0.5 \quad G_{eq} = \frac{k_1}{k_2} = 0.5 \quad R_{eq} = \frac{k_3}{k_2} = 1$$

Ejemplo 1, Dep. (G) –presa (R) , (ii)



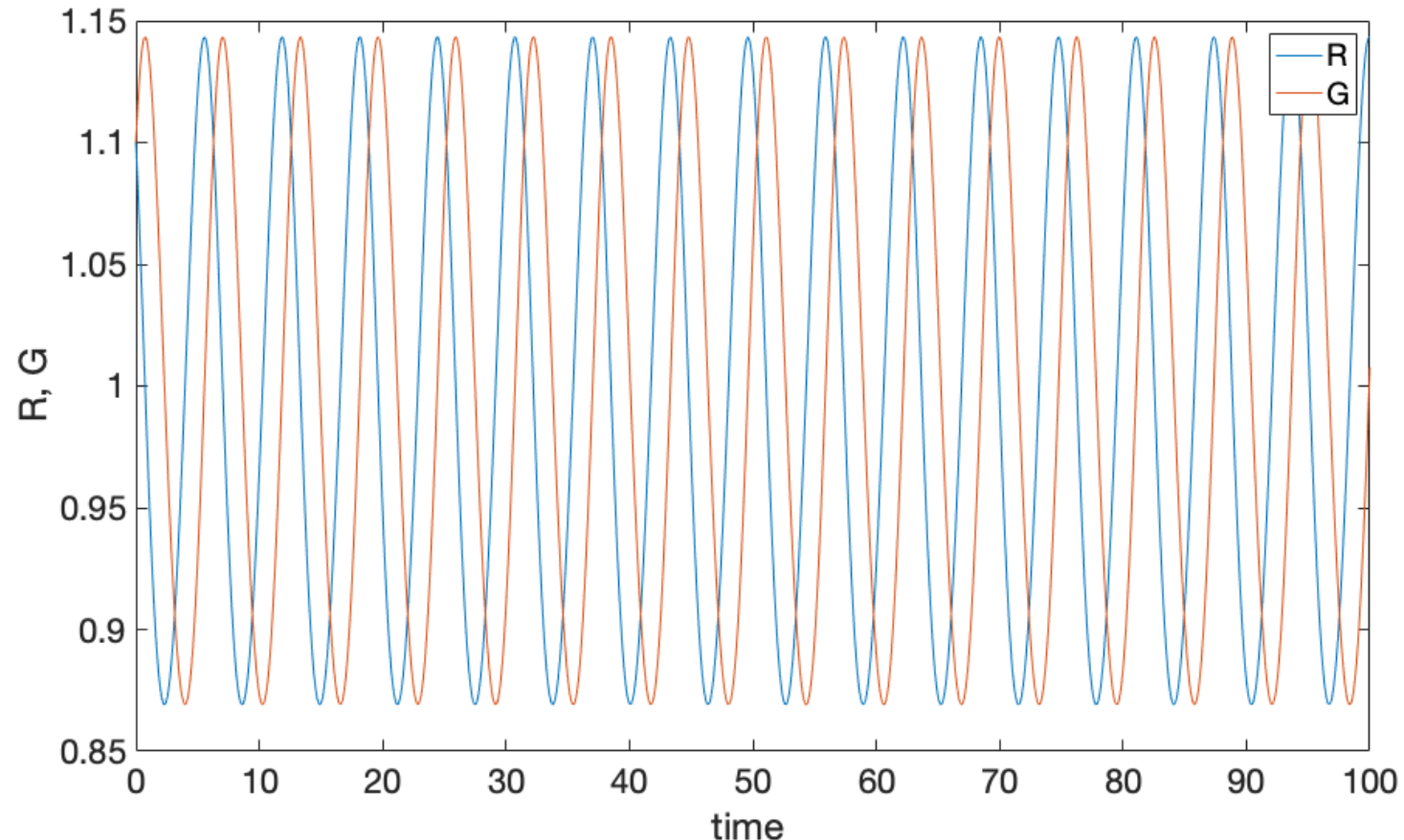
$$\text{Theoretical period : } T_{th.} = \frac{2\pi}{\sqrt{k_1 k_3}}$$

$$k_1 = 0.25; k_2 = 0.5; k_3 = 0.5$$

$$G_{eq} = \frac{k_1}{k_2} = 0.5 \quad R_{eq} = \frac{k_3}{k_2} = 1$$

Relative phase : Phase/period

Ejemplo 2, Dep. (G) –presa (R)



Here we have set the initial conditions: $G_0 = 1.1 = R_0$

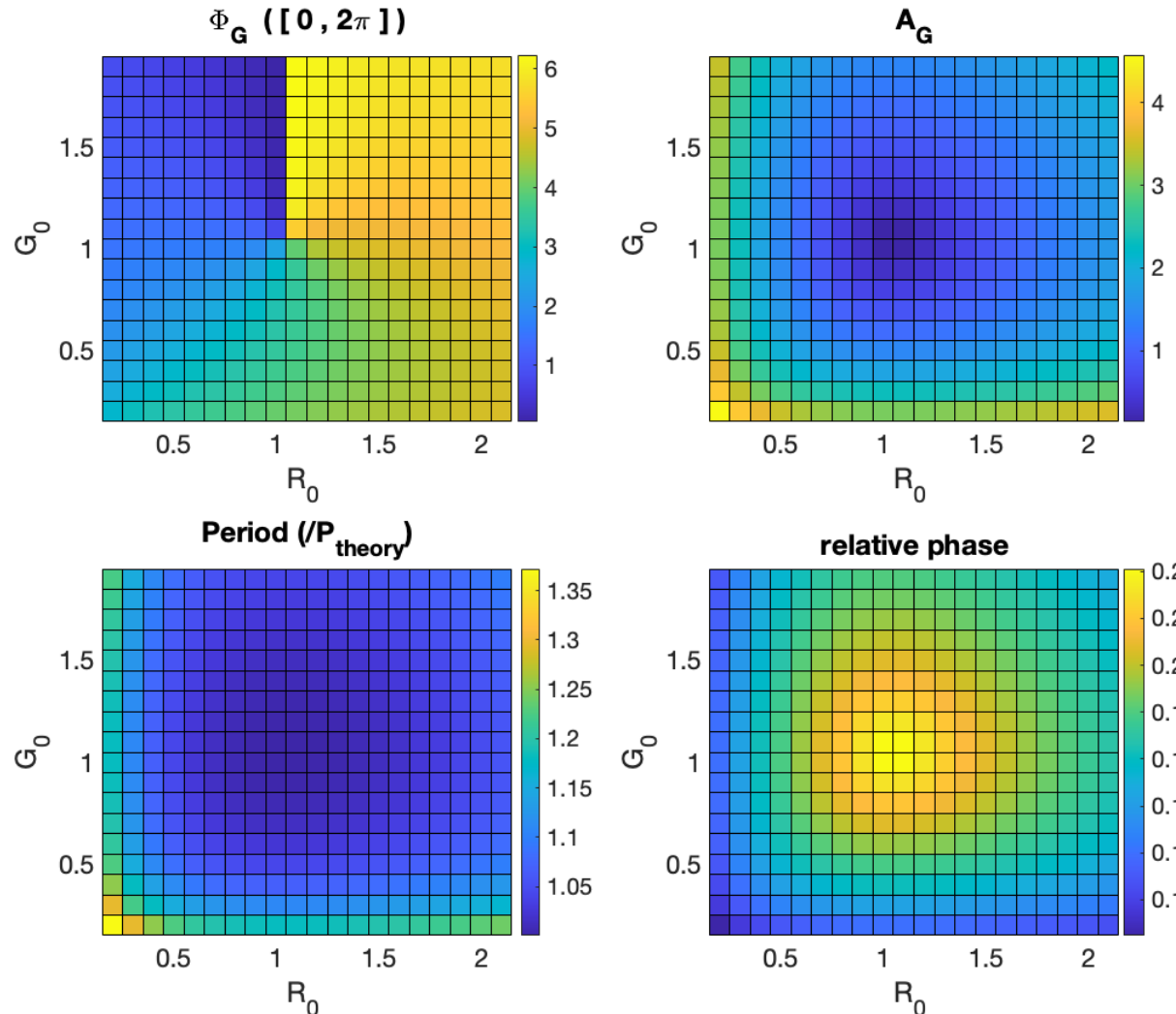
After, we will look at the influence of the initial conditions.

$$k_1 = 1; k_2 = 1; k_3 = 1$$

$$G_{eq} = \frac{k_1}{k_2} = 1$$

$$R_{eq} = \frac{k_3}{k_2} = 1$$

Ejemplo 2, Dep. (G) –presa (R) , (ii)



$$\text{Theoretical period : } T_{th.} = \frac{2\pi}{\sqrt{k_1 k_3}}$$

$$k_1 = 1; k_2 = 1; k_3 = 1$$

$$G_{eq} = \frac{k_1}{k_2} = 1$$

$$R_{eq} = \frac{k_3}{k_2} = 1$$

Relative phase : phase/period

Gap Junctions Induced Bistability Conductance in Cardiac Tissue

Jean Bragard

*Department of Physics & Applied Mathematics,
School of Sciences,
University of Navarra. 31008 Pamplona. SPAIN.*

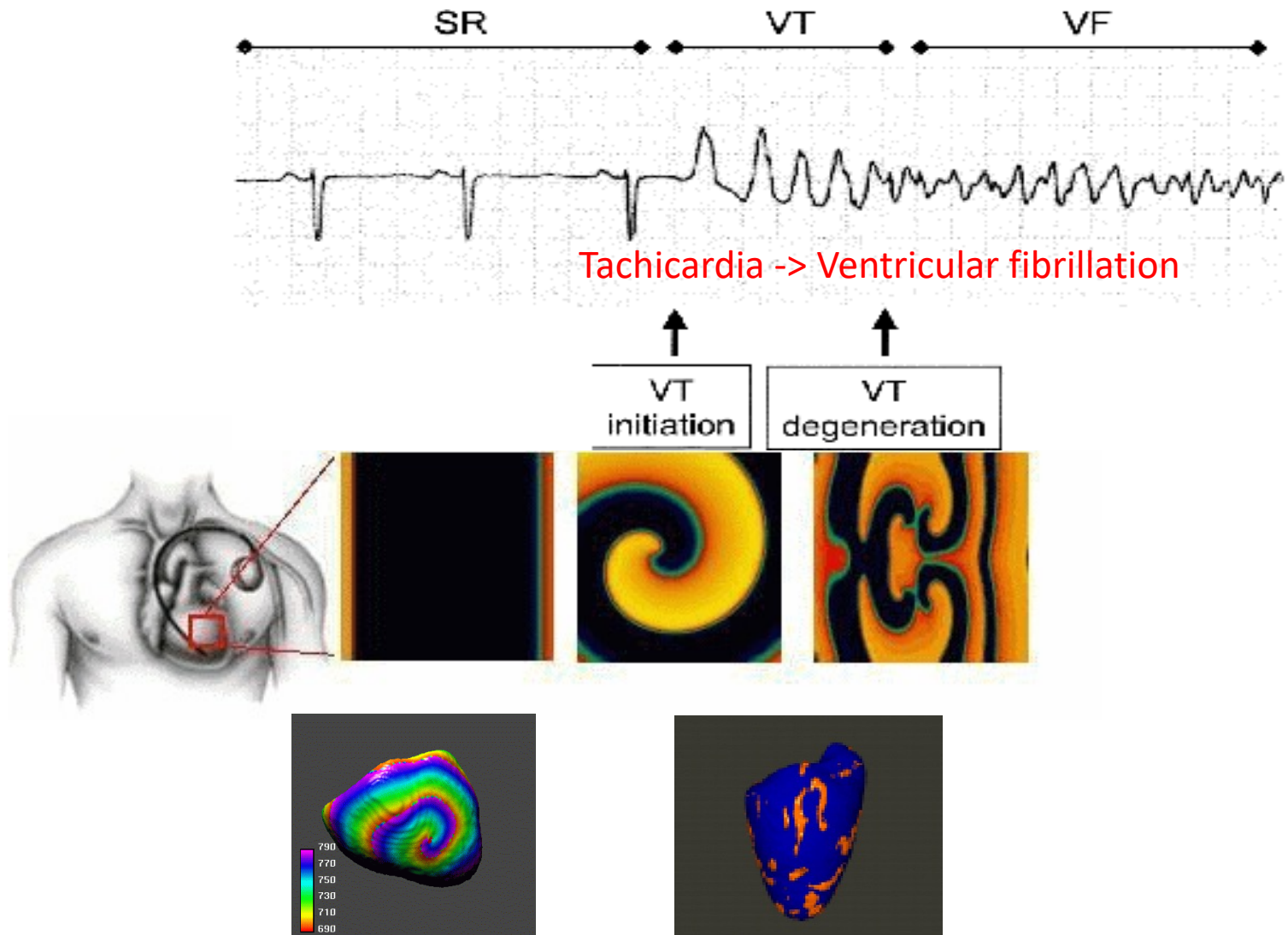


Why are we interested in studying cardiac dynamics ?

Rank ¹	Cause of death (based on ICD-10, 1992)	Number	Percent of total deaths	2005 crude death rate
...	All causes	2,448,017	100.0	825.9
1	Diseases of heart	(I00–I09, I11, I13, I20–I51) 652,091	26.6	220.0
2	Malignant neoplasms	(C00–C97) 559,312	22.8	188.7
3	Cerebrovascular diseases	(I60–I69) 143,579	5.9	48.4
4	Chronic lower respiratory diseases	(J40–J47) 130,933	5.3	44.2
5	Accidents (unintentional injuries)	(V01–X59, Y85–Y86) 117,809	4.8	39.7
6	Diabetes mellitus	(E10–E14) 75,119	3.1	25.3
7	Alzheimer's disease	(G30) 71,599	2.9	24.2
8	Influenza and pneumonia	(J10–J18) 63,001	2.6	21.3
9	Nephritis, nephrotic syndrome and nephrosis	(N00–N07, N17–N19, N25–N27) 43,901	1.8	14.8
10	Septicemia	(A40–A41) 34,136	1.4	11.5
11	Intentional self-harm (suicide)	(*U03, X60–X84, Y87.0) 32,637	1.3	11.0
12	Chronic liver disease and cirrhosis	(K70, K73–K74) 27,530	1.1	9.3
13	Essential (primary) hypertension and hypertensive renal disease	(I10, I12) 24,902	1.0	8.4
14	Parkinson's disease	(G20–G21) 19,544	0.8	6.6
15	Assault (homicide)	(*U01–*U02, X85–Y09, Y87.1) 18,124	0.7	6.1
...	All other causes (residual)	433,800	17.7	146.4

Cardiac diseases are among the leading causes of death and we should understand better all the mechanisms associated with them.

Normal electric activity may be disrupted by failures in the propagation of the action potentials



(Keener y Panfilov (1995))

